Electron bubbles and Weyl fermions in chiral superfluid ^{3}He-*A*

Oleksii Shevtsov* and J. A. Sauls†
Department of Physics and Astronomy, Northwestern University, Evanston, Illinois 60208, USA
(Received 20 June 2016; published 12 August 2016)

Electrons embedded in liquid ^{3}He form mesoscopic bubbles with large radii compared to the interatomic distance between ^{3}He atoms, voids of $N_{\rm bubble} \approx 200$ ^{3}He atoms, generating a negative ion with a large effective mass that scatters thermal excitations. Electron bubbles in chiral superfluid ^{3}He-*A* also provide a local probe of the ground state. We develop a scattering theory of Bogoliubov quasiparticles by negative ions embedded in ^{3}He-*A* that incorporates the broken symmetries of ^{3}He-*A*, particularly broken symmetries under time reversal and mirror symmetry in a plane containing the chiral axis $\hat{\mathbf{l}}$. Multiple scattering by the ion potential, combined with branch conversion scattering by the chiral order parameter, leads to a spectrum of Weyl fermions bound to the ion that support a mass current circulating the electron bubble—a mesoscopic realization of chiral edge currents in superfluid ^{3}He-*A* films. A consequence is that electron bubbles embedded in ^{3}He-*A* acquire angular momentum, $\mathbf{L} \approx -(N_{\rm bubble}/2)\hbar\hat{\mathbf{l}}$, inherited from the chiral ground state. We extend the scattering theory to calculate the forces on a moving electron bubble, both the Stokes drag and a transverse force, $\mathbf{F}_{\rm W} = \frac{e}{c}\mathbf{v}\times\mathbf{B}_{\rm W}$, defined by an effective magnetic field, $\mathbf{B}_{\rm W} \propto \hat{\mathbf{l}}$, generated by the scattering of thermal quasiparticles off the spectrum of Weyl fermions bound to the moving ion. The transverse force is responsible for the anomalous Hall effect for electron bubbles driven by an electric field reported by the RIKEN group. Our results for the scattering cross section, drag, and transverse forces on moving ions are compared with experiments and shown to provide a quantitative understanding of the temperature dependence of the mobility and anomalous Hall angle for electron bubbles in normal and superfluid ^{3}He-*A*. We also discuss our results in relation to earlier work on the theory of negative ions in superfluid ^{3}He.

DOI: 10.1103/PhysRevB.94.064511

I. INTRODUCTION

A unique feature of the chiral phase of superfluid ^{3}He, predicted early on by Anderson and Morel (AM), is that this fluid should possess a macroscopic ground-state angular momentum, $\mathbf{L} = L_z\,\hat{\mathbf{l}}$ [1–6], where $\hat{\mathbf{l}}$ is the chiral axis along which the Cooper pairs have angular momentum $\hbar$. Ground-state currents and angular momentum are signatures of broken time-reversal and parity (BTRP) derived from the orbital motion of the Cooper pairs in ^{3}He-*A*. In this paper, we discuss signatures of BTRP generated by the structure of electrons embedded in superfluid ^{3}He-*A*. An electron forms a void, a "bubble," in liquid ^{3}He-*A* that disturbs the chiral ground state [7]. We show that multiple scattering of Bogoliubov quasiparticles off the electron bubble leads to the formation of chiral fermions bound to the electron bubble, and to a ground-state angular momentum and mass current circulating each electron bubble. Indeed, the electron bubble provides a mesocopic realization of chiral edge currents in superfluid ^{3}He-*A*. A main result of the work reported here is our formulation of a transport theory for negative ions that correctly accounts for the chiral symmetry of superfluid ^{3}He-*A*. This allows us to show that the chiral structure of the electron bubble in ^{3}He-*A* provides a quantitative theory for the anomalous Hall effect reported by Ikegami *et al.* [8,9]. We start with a brief introduction intended to make the connection between ground-state currents, angular momentum, and chiral edge states in ^{3}He-*A*, with the structure of electron bubbles in ^{3}He-*A*.

The angular momentum of bulk ^{3}He-*A* has so far not been measured, perhaps in part because of variations in the literature on the magnitute of L_z (cf. Ref. [10] and references therein). McClure and Takagi (MT) obtained the result, $L_z = (N/2)\,\hbar$, for N atoms confined in a container of volume V with cylindrical symmetry, and condensed into a chiral p-wave bound state of fermion pairs. This result is independent of whether or not the ground state is a condensate of overlapping chiral Cooper pairs ($\xi \gg a$) or a Bose-Einstein condensate of tightly bound chiral molecules ($\xi \ll a$), where ξ represents the radial extent of the pair wave function, $a = 1/\sqrt[3]{n}$ is the interatomic spacing and n is the mean atomic density. While the MT result is in accord with expectations for a BEC of $N/2$ chiral molecules, the MT result for the BCS limit suggests that the currents responsible for a ground-state angular momentum of $(N/2)\hbar$ are confined on the boundary walls [10,11].

The existence of currents confined on the boundary is a natural conclusion of the bulk-boundary correspondence for a topological phase with broken time-reversal symmetry [12–14]. In the quasi-2D limit, the chiral *A* phase is fully gapped and belongs to a topological class related to that of integer quantum Hall systems [15–17]. The topology of the chiral AM state requires gapless Weyl fermions confined on the edge of a thin film of superfluid ^{3}He-*A* [17,18]. For an isolated boundary a branch of Weyl fermions disperses linearly with momentum $p_{||}$ along the boundary, i.e. $\varepsilon(p_{||}) = c\,p_{||}$, where $c = v_f\,|\Delta|/E_f \ll v_f$ is the velocity of the Weyl fermions. The asymmetry of the Weyl branch under time reversal, $\varepsilon(-p_{||}) = -\varepsilon(p_{||})$, implies the existence of a ground-state edge current derived from the occupation of the negative energy states [10,19]. For ^{3}He-*A* confined in a thin cylindrical cavity, or a film, the *chiral edge current* on the outer boundary

*oleksii.shevtsov@northwestern.edu
†sauls@northwestern.edu

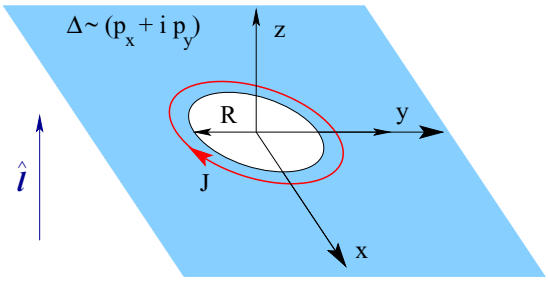

FIG. 1. An unbounded ^{3}He-A film with an inner boundary of radius $R \gg \xi_0$. A ground-state edge current of magnitude $J = \frac{1}{4} n \hbar$ circulates on the inner boundary generating an angular momentum $L_z = -(N_{\rm hole}/2)\hbar$ with $N_{\rm hole} = n\pi R^2 w$, i.e. the number of ^{3}He atoms *excluded* by the hole.

edge, $J = \frac{1}{4} n \hbar$ [20], is the source of the ground-state angular momentum, $L_z = (N/2)\hbar$, predicted by MT [10,19,21].

To reveal the edge currents, consider an unbounded thin film of superfluid ^{3}He-A with a circular barrier, a "hole," excluding ^{3}He as shown in Fig. 1. The edge current is confined to the boundary on the scale of $\xi_\Delta = \hbar v_f/2\Delta \approx 100$ nm. The angular momentum resulting from the edge current circulating the hole is $L_z = -(N_{\rm hole}/2)\hbar$, which is opposite to the chirality of the ground-state Cooper pairs, and with magnitude given by $N_{\rm hole} = n\pi R^2 w$, the number of ^{3}He atoms *excluded* by the hole of radius R and thickness w. Nature provides us with such a "hole" in the form of an electron bubble to reveal the BTRP of ^{3}He-A, and to probe the spectrum of chiral edge states, the mass current circulating the electron bubble, and the effect of the chiral edge states on the transport properties of the electron bubble in ^{3}He-A.

We begin with the structure of the electron bubble in the normal Fermi liquid phase of ^{3}He in Sec. II. The normal-state t matrix and scattering phase shifts for quasiparticles scattering off the electron bubble are central to understanding the properties of the electron bubble in superfluid ^{3}He-A. In Sec. III, we develop a scattering theory to calculate the spectrum of chiral fermions bound to the electron bubble in ^{3}He-A. We present results for the mass current and orbital angular momentum obtained from the fermionic spectrum. The momentum and energy resolved differential cross section for the scattering of Bogoliubov quasiparticles is developed in Sec. IV, and used to calculate the forces on electron bubbles moving in the chiral phase of superfluid ^{3}He.

We present new theoretical predictions and analysis for the drag force on electron bubbles in ^{3}He-A, and particularly the transverse force responsible for the anomalous Hall current of electron bubbles in superfluid ^{3}He-A. In Sec. V, we present the quantitative comparison of our theory with the measurements of the drag force and anomalous Hall effect reported by Ikegami *et al.* [8,9] Our analysis establishes that the observation of the anomalous Hall effect for negative ions is not only a signature of BTRP, but a signature of chiral fermions circulating the electron bubble.

We point out that previous theories for the mobility of ions in superfluid ^{3}He-A start from an implicit assumption of mirror symmetry in the formulation of the transport cross section for scattering of quasiparticles off the electron bubble. Specifically, in Sec. IV B and Appendix A, we discuss our theory in relation to the earlier theoretical works of Salomaa *et al.* [22] and Salmelin *et al.* [23,24], and point out that these earlier theoretical works give *zero* Hall mobility (Ref. [24]), or report a spurious Hall mobility that is an artefact of an error in evaluating the kinematics for the scattering of quasiparticles off the ion. As a result, the theory reported in Refs. [23,24] not only predicts a spurious Hall mobility in ^{3}He-A, but also a spurious anisotropic mobility in normal liquid ^{3}He.

Our formulation of the transport theory correctly accounts for the chiral symmetry of superfluid ^{3}He-A, which is at the root of the anomalous Hall effect for electrons in ^{3}He-A [25], and as shown in Sec. V C is in quantitative agreement with the experimental measurements reported in Refs. [8,9].

II. ELECTRON BUBBLES IN LIQUID ^{3}He

Electrons experience a repulsive barrier $\approx$1 eV at the surface of liquid helium [26]. When an electric field pushes the electron into helium, the combination of the barrier, the surface tension, and zero-point kinetic energy of the electron conspire to form a self-trapped electron in a spherical void of radius R, an "electron bubble" [27–30]. The basic model of an electron bubble in liquid ^{3}He is based on an energy function that consists of three terms [27,31],

$$E(R,P) = E_0(U_0,R) + 4\pi R^2\gamma + \frac{4\pi}{3}R^3 P, \qquad (1)$$

where $\gamma = 0.15$ erg/cm^2 is the surface tension of ^{3}He [32,33], P is the external pressure, and E_0 is the ground-state energy of the electron bubble trapped in an isotropic potential of radius R and depth $-U_0$. In the limit $U_0 \to \infty$, $E_0 = -U_0 + \pi^2\hbar^2/2m_e R^2$ is the energy of the electron of mass m_e in its ground state. The balance between the surface tension of liquid ^{3}He, the external pressure and the kinetic energy of the confined electron determines the bubble radius, $P = \pi\hbar^2/4m_e R^5 - 2\gamma/R$. For zero pressure, the radius is then

$$R = \left(\frac{\pi\hbar^2}{8m_e\gamma}\right)^{\frac{1}{4}} \approx 2.38\ \text{nm}\,. \qquad (2)$$

The bubble radius is large compared to the Fermi wavelength of ^{3}He quasiparticles, $\lambda_f = 1/k_f = 0.127$ nm, set by the ^{3}He density, but is small compared to the Cooper pair correlation length, $\xi_0 = \hbar v_f/2\pi k_B T_c \approx 77.3$ nm. It is useful to refer to the dimensionless ratio, $k_f R$, which for the infinte barrier limit is $k_f R = 18.67$ at $P = 0$. Models for the confining potential with a finite pressure-dependent $U_0 \sim 1$ eV yield a slightly smaller radius of $k_f R \approx 16.74$ [31].

A. Electron mobility in normal ^{3}He

A different measure of the size of the electron bubble may be obtained from the scattering of ^{3}He quasiparticles off the electron bubble, i.e. the total cross section presented to quasiparticles with momenta and energies near the Fermi surface. The scattering of quasiparticles off the heavy electron bubble determines the mobility of the electron bubble. The heavy mass of the ion and large cross section for quasiparticle collisions imply that the scattering of quasiparticles off the

electron bubble is nearly elastic [34,35]. The mobility of the electron bubble in normal ^{3}He is then temperature independent over the range $T_c < T < T_0 = \hbar^2 k_f^2/2M \approx 30$ mK, and given by

$$\frac{e}{\mu_N} = n_3 p_f \sigma_N^{tr}, \quad \sigma_N^{tr} = \int d\Omega_{\hat{\mathbf{k}}'} \frac{d\sigma}{d\Omega_{\hat{\mathbf{k}}'}} (1 - \hat{\mathbf{k}}' \cdot \hat{\mathbf{k}}), \tag{3}$$

where σ_N^{tr} is the transport cross section for elastic scattering of quasiparticles off an electron bubble, and

$$\frac{d\sigma}{d\Omega_{\hat{\mathbf{k}}'}} = \left| \frac{m^*}{2\pi\hbar^2} t_N^R(\hat{\mathbf{k}}', \hat{\mathbf{k}}; E) \right|^2 \tag{4}$$

is the differential cross section defined by the on-shell t matrix for normal-state quasiparticles with effective mass m^* scattering off a static electron bubble.

The full t matrix obeys the Lippmann-Schwinger equation, $T_N^R = V + V G_N^R T_N^R$, where G_N^R is the retarded propagator for fermions in the normal Fermi liquid. At temperatures $k_B T \ll E_f$, the properties of ^{3}He are dominated by quasiparticles with momenta near the Fermi surface, $\mathbf{k} \simeq k_f \hat{\mathbf{k}}$, and excitation energies, $\xi_{\mathbf{k}} \simeq v_f(|\mathbf{k}| - k_f)$ with $|\xi_{\mathbf{k}}| \ll E_f$. The corresponding t matrix describing the scattering of quasiparticles off the electron bubble is obtained by separating the propagator as $G_N^R = G_N^{R,low} + G_N^{R,high}$, where $G_N^{R,low} = a/(E + i0^+ - \xi_{\mathbf{k}})$ is the low-energy quasiparticle propagator with residue a, and $G_N^{R,high}$ is the high-energy, incoherent propagator. The latter renormalizes the bare ^{3}He-Ion interaction, $U = V + V G_N^{R,high} U$. The resulting t matrix, $\langle \mathbf{k}' | T_N^R | \mathbf{k} \rangle \equiv t_N^R(\hat{\mathbf{k}}', \hat{\mathbf{k}}; E)$, for elastic scattering of low-energy quasiparticles with energy E, and momenta $\mathbf{k} = k_f \hat{\mathbf{k}}$ to $\mathbf{k}' = k_f \hat{\mathbf{k}}'$ on the Fermi surface is then

$$t_N^R(\hat{\mathbf{k}}', \hat{\mathbf{k}}; E) = u(\hat{\mathbf{k}}', \hat{\mathbf{k}}) + N_f \int \frac{d\Omega_{\mathbf{k}''}}{4\pi} u(\hat{\mathbf{k}}', \hat{\mathbf{k}}'') g_N^R(\hat{\mathbf{k}}'', E)\, t_N^R(\hat{\mathbf{k}}'', \hat{\mathbf{k}}; E), \tag{5}$$

where $N_f = m^* k_f/2\pi^2\hbar^2$ is the single-spin density of states at the Fermi surface, $m^* = p_f/v_f$ is the quasiparticle effective mass, $g_N^R(\hat{\mathbf{k}}, E) = \frac{1}{a}\int d\xi_{\mathbf{k}}\, G_N^{R,low}(\mathbf{k}, E) = -i\pi$ is the quasiclassical progragator, and $u(\mathbf{k}', \mathbf{k}) = \langle \mathbf{k}' | U | \mathbf{k} \rangle$. For a spherically symmetric electron bubble, the quasiparticle-ion interaction and the t matrix can be expanded as $u(\hat{\mathbf{k}}', \hat{\mathbf{k}}) = \sum_{l \geq 0}(2l + 1)\, u_l\, P_l(\hat{\mathbf{k}}' \cdot \hat{\mathbf{k}})$, and similarly for $t_N^R(\hat{\mathbf{k}}', \hat{\mathbf{k}})$, where $\{P_l(x) \,|\, l = 0, 1, 2, \ldots\}$ is the complete set of Legendre polynomials. Using the convolution integral, $\int \frac{d\Omega_{\mathbf{k}''}}{4\pi} P_{l'}(\hat{\mathbf{k}}' \cdot \hat{\mathbf{k}}'') P_l(\hat{\mathbf{k}}'' \cdot \hat{\mathbf{k}}) = \delta_{ll'} P_l(\hat{\mathbf{k}}' \cdot \hat{\mathbf{k}})/(2l + 1)$, we obtain $t_l^R(E) = u_l/(1 + i\pi N_f u_l)$. The structure of the t matrix can be encoded in the scattering phases shifts, δ_l, defined in terms of the strength of the quasiparticle-ion potential in each angular momentum channel, u_l, and the density of states, N_f; $\tan\delta_l = -\pi N_f u_l$, with the t matrix expressed as

$$t_N^R(\hat{\mathbf{k}}', \hat{\mathbf{k}}; E) = -\frac{1}{\pi N_f} \sum_{l=0}^{\infty} (2l + 1) e^{i\delta_l} \sin\delta_l\, P_l(\hat{\mathbf{k}}' \cdot \hat{\mathbf{k}}). \tag{6}$$

Integrating Eq. (4) over all scattering directions, we obtain the standard result for the total cross section [36]

$$\sigma_N = \frac{4\pi}{k_f^2} \sum_{l=0}^{\infty} [(2l + 1) \sin^2\delta_l]. \tag{7}$$

Similarly, the transport cross section is determined by the set of scattering phase shifts that parametrize the quasiparticle-ion potential:

$$\sigma_N^{tr} = \frac{4\pi}{k_f^2} \sum_{l=0}^{\infty} [(2l + 1) \sin^2\delta_l - 2(l + 1) \cos(\delta_{l+1} - \delta_l) \sin\delta_{l+1} \sin\delta_l]. \tag{8}$$

B. Hard-sphere scattering of quasiparticles

The structure of the electron bubble as a spherical void of displaced ^{3}He suggests the model of a short-range repulsive barrier preventing penetration of ^{3}He into the bubble. The potential barrier, $V_0 \approx 1$ eV, is very large compared to typical quasiparticle kinetic energies, suggesting a reasonable model for the quasiparticle-ion potential is a single parameter hard-sphere potential parametrized by barrier radius R. The scattering phase shifts that define the quasiparticle-ion t matrix for hard-sphere scattering are calculated in standard textbooks [36]:

$$\tan\delta_l = \frac{j_l(k_f R)}{n_l(k_f R)}, \tag{9}$$

where $j_l(x)$ and $n_l(x)$ are order l spherical Bessel functions of the first and second kind, respectively.

Figure 2 shows the set of phase shifts for a hard sphere with a ratio of radius to Fermi wavelength of $k_f R = 11.17$. Note that for channels with $l \gtrsim k_f R$, the phase shift decreases rapidly to zero. The radius is determined by requiring the transport cross section computed for the hard-sphere potential reproduce the measured normal-state ion mobility according to Eqs. (3), (8), and (9). At $P = 0$ bar, the Fermi wave number, $k_f = 7.853\,\text{nm}^{-1}$, determines the Fermi momentum, $p_f = \hbar k_f$, and

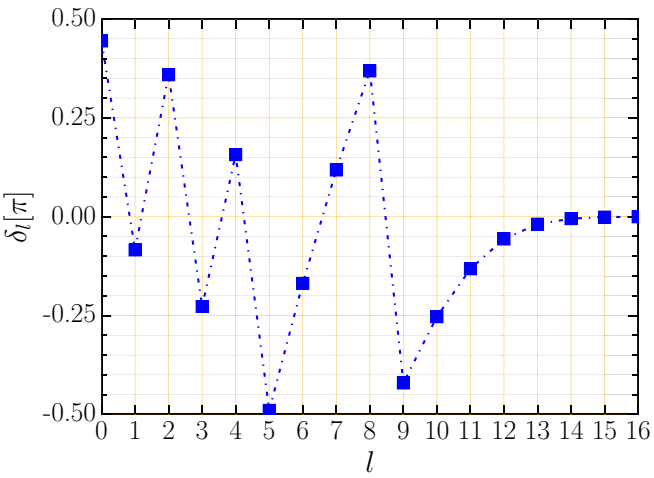

FIG. 2. Phase shifts as a function of angular momentum channel number l for the hard-sphere potential with $k_f R = 11.17$. Note that channels with $l > 12$ are effectively irrelevant.

particle density, $n_3 = k_f^3/3\pi^2$. Combined with the measured normal-state mobility, $\mu_N^{\rm exp} = 1.7\times10^{-6}\,{\rm m}^2/{\rm V\,s}$ [8], we obtain $k_f R = 11.17$, smaller than the bubble radius determined by the surface tension and zero-point kinetic energy of the electron. For scattering of quasiparticles off the electron bubble, this is the relevant measure of the size of the electron bubble [37]. In what follows, we develop the theory for the structure of the electron bubble in a chiral superfluid ^{3}He-A based on multiple scattering of Bogoliubov quasiparticles off the negative ion.

III. STRUCTURE OF AN ELECTRON BUBBLE IN ^{3}He-A

The structure of an electron bubble in ^{3}He-A is much richer than that in normal ^{3}He. However, multiple scattering channels of electron bubbles are central in determining the spectrum of chiral fermions confined near the electron bubble. Here we develop the theory for Bogoliubov quasiparticles scattering off an electron bubble embedded in superfluid ^{3}He-A, and use the scattering theory to calculate the local spectrum of chiral fermions bound to the electron bubble, as well as the mass current and angular momentum circulating the electron bubble. Our formulation parallels Refs. [22,24,38,39]; however, we incorporate broken parity and time reversal, in addition to broken U(1) and SO(3) symmetries, of the ground state of ^{3}He-A in our formulation of the scattering of quasiparticles off electron bubbles.

Fermionic excitations of superfluid ^{3}He-A are coherent superpositions of normal-state particles and holes described by four-component Bogoliubov-Nambu spinor wave functions, $\Psi(\mathbf{r}) = (u_\uparrow(\mathbf{r}),u_\downarrow(\mathbf{r}),v_\downarrow(\mathbf{r}),v_\uparrow(\mathbf{r}))^{\rm T}$, that are solutions of Bogoliubov's equations

$$\widehat{H}_S\Psi(\mathbf{r}) = E\Psi(\mathbf{r}), \quad \widehat{H}_S = \begin{pmatrix} \hat{H}_N & \hat{\Delta}(\mathbf{p}) \\ \hat{\Delta}^\dagger(\mathbf{p}) & -\hat{H}_N \end{pmatrix}, \tag{10}$$

$$\hat{H}_N = \left(\frac{\mathbf{p}^2}{2m^*} - \mu\right)\mathbb{1}, \quad \hat{\Delta}(\mathbf{p}) = \sigma_x\Delta(\mathbf{p}_x + i\mathbf{p}_y)/p_f, \tag{11}$$

where $\hat{\Delta}(\mathbf{p})$ is the mean-field pairing potential (order parameter) responsible for particle-hole coherence of the fermionic excitations, and for branch conversion scattering between particlelike and holelike Bogoliubov quasiparticles. Note that $\mathbf{p} = -i\hbar\nabla$, $\mathbb{1}$ is the unit matrix in spin space, and σ_x is the Pauli matrix describing the equal-spin pairing state (ESP) of Cooper pairs with spin projections $S_x = \pm1$; equivalently, the Cooper pairs have zero spin projection along $\hat{\mathbf{z}}$. The chiral axis $\hat{\mathbf{l}}$ for A-phase Cooper pairs are also along $\hat{\mathbf{z}}$. Thus the 4×4 equation splits into a pair of two-component equations for $\Psi_\uparrow = (u_\uparrow,0,0,v_\uparrow)^{\rm T}$ and $\Psi_\downarrow = (0,u_\downarrow,v_\downarrow,0)^{\rm T}$.

A. Scattering states and propagators

The scattering states are Bogoliubov quasiparticles in homogeneous ^{3}He-A, i.e. far from the electron bubble, in which case the orbital part of the mean-field pairing potential can be expressed as $\Delta(\hat{\mathbf{k}}_x + i\hat{\mathbf{k}}_y) = \Delta\sin\theta\, e^{+i\phi}$, where θ is the polar angle of the relative momentum of the Cooper pairs in momentum space and the azimuthal angle, ϕ, is the phase of the Cooper pairs in momentum space that winds by 2π about the chiral axis, $\hat{\mathbf{l}}$. This phase winding plays a central role in the scattering of quasiparticles off the electron bubble embedded in ^{3}He-A. The scattering states are eigenstates of momentum, $\mathbf{p}|\,\mathbf{k}\,\rangle = \hbar\mathbf{k}\,|\,\mathbf{k}\,\rangle$. There are four Bogoliubov quasiparticle states for each energy - particlelike and holelike excitations each with two degenerate spin states. The Bogoliubov-Nambu spinors for the scattering states have the form

$$|\Psi_{1,\mathbf{k}\sigma}\rangle = \begin{pmatrix} u_\mathbf{k}\chi_\sigma \\ -v_\mathbf{k}^*\chi_{\bar\sigma} \end{pmatrix} \otimes |\mathbf{k}\rangle = |\Phi_{1,\mathbf{k}\sigma}\rangle \otimes |\mathbf{k}\rangle\,, \tag{12}$$

$$|\Psi_{2,\mathbf{k}\sigma}\rangle = \begin{pmatrix} v_\mathbf{k}\chi_\sigma \\ -u_\mathbf{k}^*\chi_{\bar\sigma} \end{pmatrix} \otimes |\mathbf{k}\rangle = |\Phi_{2,\mathbf{k}\sigma}\rangle \otimes |\mathbf{k}\rangle, \tag{13}$$

where the particle and hole amplitudes are given by

$$u_\mathbf{k} = \frac{1}{\sqrt{2}}\sqrt{1 + \frac{\xi_k}{E_\mathbf{k}}}\,, \quad v_\mathbf{k} = \frac{1}{\sqrt{2}}\sqrt{1 - \frac{\xi_k}{E_\mathbf{k}}}\,e^{i\phi}\,, \tag{14}$$

$$\langle\mathbf{r}|\mathbf{k}\rangle = e^{i\mathbf{k}\mathbf{r}}\,, \quad \chi_\uparrow = \begin{pmatrix}1\\0\end{pmatrix}, \quad \chi_\downarrow = \begin{pmatrix}0\\1\end{pmatrix}, \quad \chi_{\bar\uparrow} = \chi_\downarrow, \tag{15}$$

where $E_\mathbf{k} = \sqrt{\xi_\mathbf{k}^2 + |\Delta(\hat{\mathbf{k}})|^2}$ is the excitation energy for Bogoliubov quasiparticles. The spinors, $|\Psi_{1,\mathbf{k}\sigma}\rangle$, are the particlelike states with $\xi_k > 0$ and group velocity $\nabla_\mathbf{k}E_\mathbf{k} > 0$, while $|\Psi_{2,\mathbf{k}\sigma}\rangle$ are the holelike states with $\xi_k < 0$ and $\nabla_\mathbf{k}E_\mathbf{k} < 0$. Note that the winding number of the Cooper pairs is imprinted as a relative phase between the particle- and holelike amplitudes in Eq. (14).

The causal propagator is the retarded Green's function of Bogoliubov's equations, $(\varepsilon\widehat{1} - \widehat{H}_{\rm S})\,\widehat{G}_{\rm S}^{\rm R} = \widehat{1}$, with $\varepsilon = E + i\eta$ ($\eta \to 0^+$), which for the bulk excitations in the homogeneous A phase is given by

$$\widehat{G}_{\rm S}^{\rm R}(\mathbf{k},E) = \frac{1}{\varepsilon^2 - E_\mathbf{k}^2}\begin{pmatrix} (\varepsilon+\xi_k)\mathbb{1} & -\hat{\Delta}(\hat{\mathbf{k}}) \\ -\hat{\Delta}^\dagger(\hat{\mathbf{k}}) & (\varepsilon-\xi_k)\mathbb{1}\end{pmatrix}. \tag{16}$$

Note that $\widehat{G}_{\rm S}^{\rm R}(\mathbf{k},E)$ is restricted to the low-energy region of the Fermi surface where the normal-state is well described by long-lived quasiparticles. The corresponding Nambu matrix for the normal-state propagator,

$$\widehat{G}_{\rm N}^{\rm R}(\mathbf{k},E) = \begin{pmatrix} (\varepsilon-\xi_k)^{-1}\mathbb{1} & 0 \\ 0 & (\varepsilon+\xi_k)^{-1}\mathbb{1}\end{pmatrix}, \tag{17}$$

includes both the particle- and hole propagators.

B. T matrix

The electron bubble introduces a strong, short-range potential that scatters Bogoliubov quasiparticles. The t matrix is given by the Lippmann-Schwinger equation, which becomes a 4×4 Nambu matrix whose elements define the transition amplitudes for scattering of Bogoliubov particles and holes, including branch conversion, i.e. Andreev scattering,

$$\widehat{T}_{\rm S} = \widehat{V} + \widehat{V}\widehat{\mathscr{G}}_{\rm S}^{\rm R}\widehat{T}_{\rm S}, \quad \text{where} \quad \widehat{V} = \begin{pmatrix} V(\mathbf{r}) & 0 \\ 0 & -V(\mathbf{r})\end{pmatrix}, \tag{18}$$

is the Nambu matrix for the ion potential, and $\widehat{\mathscr{G}}_{\rm S}^{\rm R}$ is the exact propagator in the presence of the local potential of the ion. For an ion with small cross section on the scale of the size of Cooper pairs, we are justified in replacing $\widehat{\mathscr{G}}_{\rm S}^{\rm R} \to \widehat{G}_{\rm S}^{\rm R}$, i.e. the bulk propagator in the absence of the ion given by Eq. (16). We can use the corresponding Lippman-Schwinger equation

for scattering of quasiparticles in the normal state to eliminate the ion potential $\hat{V}$ in favor of the normal-state t matrix [40],

$$\widehat{T}_S = \widehat{T}_N + \widehat{T}_N\big(\widehat{G}_S^R - \widehat{G}_N^R\big)\widehat{T}_S\,. \tag{19}$$

The normal state t matrix can be expressed in terms of the quasiparticle t matrix and has the diagonal form in Nambu space,

$$\widehat{T}_{\rm N}(\hat{\mathbf{k}}',\hat{\mathbf{k}}) = \begin{pmatrix} t_{\rm N}^{\rm R}(\hat{\mathbf{k}}',\hat{\mathbf{k}})\mathbb{1} & 0 \\ 0 & -\big[t_{\rm N}^{\rm R}(-\hat{\mathbf{k}}',-\hat{\mathbf{k}})\mathbb{1}\big]^\dagger \end{pmatrix}. \tag{20}$$

The ground state of ^{3}He-A breaks rotational symmetry, but preserves axial rotations combined with a compensating gauge transformation. Thus scattering of quasiparticles off the electron bubble in ^{3}He-A no longer separates into angular momentum channels with a precise l. However, the projection of the angular mometum, labeled by m, is conserved for nonbranch conversion scattering, and changes by one unit of angular momentum for branch conversion scattering. Thus, in reducing the t matrix for the scattering of Bogoliubov quasiparticles in ^{3}He-A, it is convenient to rewrite Eq. (6) as an expansion in azimuthal harmonics by using the addition theorem to express the Legendre functions in terms of the spherical harmonics [41]. We then change the order of the summations over l and m,

$$t_N(\hat{\mathbf{k}}',\hat{\mathbf{k}}) = -\frac{1}{\pi N_F}\sum_{m=-\infty}^{\infty} t_N^m(u',u)e^{-im(\phi'-\phi)},$$

$$t_N^m(u',u) = 4\pi\sum_{l=|m|}^{\infty} e^{i\delta_l}\sin\delta_l\,\Theta_l^m(u')\Theta_l^m(u), \tag{21}$$

where (θ,ϕ) $[(\theta',\phi')]$ are spherical coordinates of $\hat{\mathbf{k}}$ $[\hat{\mathbf{k}}']$ in momentum space, with $u\equiv\cos\theta$ and $u'\equiv\cos\theta'$. The functions $\Theta_l^m(\cos\theta)$ are spherical harmonics with the phase winding removed, i.e. $Y_l^m(\theta,\phi) = \Theta_l^m(\cos\theta)\,e^{im\phi}$.

For elastic scattering of Bogoliubov quasiparticles, we can reduce Eq. (19) to a linear integral equation with $\widehat{T}_{\rm N}^{\rm R}(\hat{\mathbf{k}}',\hat{\mathbf{k}})$ as the source term [42]:

$$\widehat{T}_{\rm S}^{\rm R}(\hat{\mathbf{k}}',\hat{\mathbf{k}};E) = \widehat{T}_{\rm N}^{\rm R}(\hat{\mathbf{k}}',\hat{\mathbf{k}}) + N_f\int\frac{d\Omega_{\mathbf{k}''}}{4\pi} \times \widehat{T}_{\rm N}^{\rm R}(\hat{\mathbf{k}}',\hat{\mathbf{k}}'')\big[\widehat{g}_{\rm S}^{\rm R}(\hat{\mathbf{k}}'',E) - \widehat{g}_{\rm N}^{\rm R}(\hat{\mathbf{k}}'',E)\big]\widehat{T}_{\rm S}^{\rm R}(\hat{\mathbf{k}}'',\hat{\mathbf{k}};E), \tag{22}$$

where the propagators in Eq. (22) are confined to a narrow shell of energies and momenta near the Fermi surface and evaluated in the quasiclassical approximation [43],

$$\widehat{g}_{\rm S}^{\rm R}(\hat{\mathbf{k}}'',E) = -\frac{\pi}{\sqrt{|\Delta(\hat{\mathbf{k}})|^2-\varepsilon^2}}\begin{pmatrix} \varepsilon\mathbb{1} & -\hat{\Delta}(\hat{\mathbf{k}}) \\ -\hat{\Delta}^\dagger(\hat{\mathbf{k}}) & \varepsilon\mathbb{1}\end{pmatrix}. \tag{23}$$

The corresponding normal-state quasiclassical propagator is $\widehat{g}_{\rm N}^{\rm R}(\mathbf{k},E) = -i\pi\widehat{1}$. For scattering off an electron bubble in ^{3}He-A the quasiclassical t matrix reduces to a set of 4×4 matrix equations for scattering amplitudes, t_a^m for Nambu components, $a = 1,2,3,4$, for each angular momentum quantum number, $m\in\{0\pm1,\pm2,\ldots\}$. In particular, we parametrize $\widehat{T}_{\rm S}^{\rm R}$ as

$$\widehat{T}_{\rm S}^{\rm R} = \begin{pmatrix} t_1(\hat{\mathbf{k}}',\hat{\mathbf{k}};E)\mathbb{1} & t_2(\hat{\mathbf{k}}',-\hat{\mathbf{k}};E)\sigma_x \\ t_3(-\hat{\mathbf{k}}',\hat{\mathbf{k}};E)\sigma_x & t_4(-\hat{\mathbf{k}}',-\hat{\mathbf{k}};E)\mathbb{1}\end{pmatrix} = \frac{-1}{\pi N_F}\sum_{m=-\infty}^{\infty} e^{-im(\phi'-\phi)}\begin{pmatrix} t_1^m(u',u)\mathbb{1} & (-1)^m e^{i\phi'}t_2^m(u',-u)\sigma_x \\ (-1)^{m+1}e^{-i\phi'}t_3^m(-u',u)\sigma_x & t_4^m(-u',-u)\mathbb{1}\end{pmatrix}. \tag{24}$$

The prefactors $(-1)^m$ in Eq. (24) reflect the sign changes for branch conversion scattering, i.e. $\hat{\mathbf{k}}\to-\hat{\mathbf{k}}$ is equivalent to $(\theta\to\pi-\theta,\phi\to\pi+\phi)$. The factors of $\exp(\pm i\phi')$ in the off-diagonal terms reflect the phase winding of the order parameter. This parametrization reduces the matrix integral equation to a set of coupled one-dimensional integral equations for $t_a^m(u',u)$,

$$t_1^m(u',u) = t_N^m(u',u) + \int_{-1}^{1}\frac{du''}{2}t_N^m(u',u'')\big[\mathfrak{G}^{\rm R}(\hat{\mathbf{k}}'',\varepsilon)t_1^m(u'',u) + (-1)^m e^{-i\phi''}\mathfrak{F}^{\rm R}(\hat{\mathbf{k}}'',\varepsilon)t_3^m(-u'',u)\big], \tag{25}$$

$$t_3^m(-u',u) = -\int_{-1}^{1}\frac{du''}{2}t_N^{m+1}(u',u'')^*\big[\mathfrak{G}^{\rm R}(\hat{\mathbf{k}}'',\varepsilon)t_3^m(-u'',u) + (-1)^m e^{i\phi''}\mathfrak{F}^{\rm R}(\hat{\mathbf{k}}'',\varepsilon)^*t_1^m(u'',u)\big], \tag{26}$$

$$t_2^m(u',-u) = \int_{-1}^{1}\frac{du''}{2}t_N^{m-1}(u',u'')\big[\mathfrak{G}^{\rm R}(\hat{\mathbf{k}}'',\varepsilon)t_2^m(u'',-u) + (-1)^{m+1}e^{-i\phi''}\mathfrak{F}^{\rm R}(\hat{\mathbf{k}}'',\varepsilon)t_4^m(-u'',-u)\big], \tag{27}$$

$$t_4^m(-u',-u) = -t_N^m(u',u)^* - \int_{-1}^{1}\frac{du''}{2}t_N^m(u',u'')^*\big[\mathfrak{G}^{\rm R}(\hat{\mathbf{k}}'',\varepsilon)t_4^m(-u'',-u) + (-1)^{m+1}e^{i\phi''}\mathfrak{F}^{\rm R}(\hat{\mathbf{k}}'',\varepsilon)^*t_2^m(u'',-u)\big], \tag{28}$$

where

$$\mathfrak{G}^{\rm R}(\hat{\mathbf{k}},\varepsilon) = \frac{\varepsilon}{\sqrt{|\Delta(\hat{\mathbf{k}})|^2-\varepsilon^2}} - i, \tag{29}$$

$$\mathfrak{F}^{\rm R}(\hat{\mathbf{k}},\varepsilon) = \frac{\Delta(\hat{\mathbf{k}})}{\sqrt{|\Delta(\hat{\mathbf{k}})|^2-\varepsilon^2}}. \tag{30}$$

Note that $t_1^m(u',u)$ is the scattering amplitude for quasiparticle excitations with angular momentum projection m, while $t_4^m(u',u)$ is the corresponding quasihole amplitude. Branch conversion scattering, generated by the anomalous propagator, $\mathfrak{F}^{\rm R}(\hat{\mathbf{k}},\varepsilon)$, is given by the amplitudes $t_2^m(u',-u)$ (hole $\to$ particle) and $t_3^m(-u',u)$ (particle $\to$ hole). Multiple scattering couples these amplitudes in pairs, $\{t_1^m,t_3^m\}$ and $\{t_2^m,t_4^m\}$ as indicated in Eqs. (25)–(28). The sets of equations are solved

numerically. In Sec. IV, the solution to the t matrix is used to calculate the differential cross section for the scattering of Bogoliubov quasiparticles off the electron bubble, and from that the forces on electron bubbles moving in response to an external electric field.

C. Local density of states

We first use the t matrix to calculate the spectrum of chiral fermions bound to the electron bubble. The asymmetry in the spectrum with respect to the orbital quantum number is responsible for the ground state current and angular momentum bound to the electron bubble. The Nambu Green's function determines the local density of states,

$$N(\mathbf{r},E) = -\frac{1}{2\pi}\mathrm{Im}\big\{\mathrm{Tr}\big[\widehat{\mathscr{G}}^{\mathrm{R}}_{\mathrm{S}}(\mathbf{r},\mathbf{r};E)\big]\big\}\,, \tag{31}$$

where the trace is over both particle-hole and spin space, and $\widehat{\mathscr{G}}^{\mathrm{R}}_{\mathrm{S}}(\mathbf{r}',\mathbf{r};E)$ is the retarded Green's function in the presence of an electron bubble. It is convenient to express $\widehat{\mathscr{G}}^{\mathrm{R}}_{\mathrm{S}}(\mathbf{r}',\mathbf{r};E)$ in momentum space,

$$\mathscr{G}^{\mathrm{R}}_{\mathrm{S}}(\mathbf{r}',\mathbf{r};E) = \int\frac{d^3k}{(2\pi)^3}\int\frac{d^3k'}{(2\pi)^3}e^{i(\mathbf{k}'\cdot\mathbf{r}'-\mathbf{k}\cdot\mathbf{r})}\mathscr{G}^{\mathrm{R}}_{\mathrm{S}}(\mathbf{k}',\mathbf{k};E). \tag{32}$$

The low-energy Nambu Green's function for quasiparticles and pairs in the presence of the ion potential can be expressed in terms of the bulk propagator and the quasiparticle-ion t matrix,

$$\begin{aligned}\widehat{\mathscr{G}}^{\mathrm{R}}_{\mathrm{S}}(\mathbf{k}',\mathbf{k};E) &= (2\pi)^3\delta(\mathbf{k}'-\mathbf{k})\,\widehat{G}^{\mathrm{R}}_{\mathrm{S}}(\mathbf{k},E)\\ &\quad+\widehat{G}^{\mathrm{R}}_{\mathrm{S}}(\mathbf{k}',E)\widehat{T}^{\mathrm{R}}_{\mathrm{S}}(\mathbf{k}',\mathbf{k};E)\widehat{G}^{\mathrm{R}}_{\mathrm{S}}(\mathbf{k},E).\end{aligned} \tag{33}$$

For energies $|E|\ll E_f$, we can evaluate the t matrix and propagators in the quasiclassical approximation and obtain an explicit expression for the local density of states (LDOS).

Figure 3 shows the local density of states calculated at the position, $r = 30\,k_f^{-1}$ and $\vartheta=\pi/2$, i.e. approximately 19 Fermi wavelengths from the surface of the electron bubble. The bulk density of states is shown as the dashed line. A van Hove singularity occurs at the maximum gap in the bulk excitation spectrum, while the low-energy spectrum results from the nodal quasiparticles near $\theta=0,\pi$. Multiple scattering, both potential and branch conversion, by the ion and the chiral order parameter generates Andreev bound states

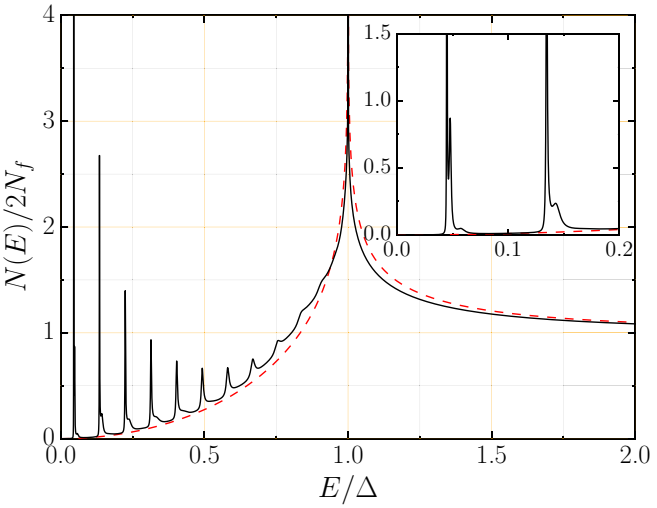

FIG. 3. Local quasiparticle density of states around an electron bubble in superfluid ^{3}He-A at distance $r = 30\,k_f^{-1}$ from the center of the bubble, and in the equatorial plane, i.e. polar angle $\vartheta=\pi/2$ relative to the chiral axis. The bubble is described as a hard sphere with radius $R = 11.17\,k_f^{-1}$. The inset shows two low-energy resonances with internal structure in their spectral density.

indexed by the angular momentum channel, m, and linear momentum, $p_z = p_f\cos\theta$. The bound states are broadened into low-energy bands by integration over p_z, and then into resonances by hybridization with the continuum of nodal quasiparticles. There are $l_{\max}\approx k_f R\approx 12$ subgap resonances shown in Fig. 3.

More detailed spectral information is obtained by resolving the LDOS in angular momentum channels. The reduction of the t matrix as a sum over amplitudes with well defined angular momentum projection implies a similar chiral decomposition of the LDOS,

$$N(\mathbf{r},E) = N_0(E) + \sum_{m=-\infty}^{\infty}\delta N_m(\mathbf{r},E)\,, \tag{34}$$

where $N_0(E)$ is the bulk density of states in superfluid ^{3}He-A

$$N_0(E) = N_F\frac{|E|}{\Delta}\ln\left|\frac{|E|+\Delta}{|E|-\Delta}\right|, \tag{35}$$

and $\delta N_m(\mathbf{r},E)$, obtained from Eqs. (31)–(33) with the solutions of Eqs. (25)–(28), is given by

$$\delta N_m(\mathbf{r},E) = 4\pi^2 N_f\,\mathrm{Im}\left\{\sum_{l,l'=|m|}^{\infty}\Theta^m_{l'}(v)\Theta^m_l(v)\int_{-1}^{1}du'\Theta^m_{l'}(u')e^{-\sqrt{\Delta^2(1-u'^2)-\varepsilon^2}\frac{r}{\hbar v_f}}\int_{-1}^{1}du\,\Theta^m_l(u)e^{-\sqrt{\Delta^2(1-u^2)-\varepsilon^2}\frac{r}{\hbar v_f}}K^m_{l'l}(u',u,\varepsilon)\right\}, \tag{36}$$

where $u=\cos\theta$ and $u'=\cos\theta'$ in momentum space, $\mathbf{r}=(r,\vartheta,\varphi)$ is the spatial coordiate in spherical coordinates with $v=\cos\vartheta$, and the matrix elements, $K^m_{ll'}$, are given in terms of spherical Bessel functions, the intermediate propagator and the elements of the t matrix [see Appendix B for details leading to Eq. (37)],

$$\begin{aligned}K^m_{l'l}(u',u,\varepsilon) = i^{l'-l}\Bigg\{&\frac{j_{l'}(k_Fr)j_l(k_Fr)}{\sqrt{\Delta^2(1-u'^2)-\varepsilon^2}\sqrt{\Delta^2(1-u^2)-\varepsilon^2}}\Big[\Delta^2\sqrt{1-u'^2}\sqrt{1-u^2}\big(t_1^{m-1}+t_4^{m+1}\big)+\varepsilon^2\big(t_1^m+t_4^m\big)\\ &+(-1)^m\Delta\varepsilon\sqrt{1-u'^2}\big(t_3^m-t_2^m\big)+(-1)^m\Delta\varepsilon\sqrt{1-u^2}\big(t_2^{m+1}-t_3^{m-1}\big)\Big]+n_{l'}(k_Fr)n_l(k_Fr)\big(t_1^m+t_4^m\big)\end{aligned}$$

$$- \frac{j_{l'}(k_F r) n_l(k_F r)}{\sqrt{\Delta^2(1-u'^2)-\varepsilon^2}} \left[\varepsilon\left(t_1^m - t_4^m\right) + (-1)^m \Delta \sqrt{1-u'^2}\left(t_2^m + t_3^m\right)\right]$$

$$- \frac{n_{l'}(k_F r) j_l(k_F r)}{\sqrt{\Delta^2(1-u^2)-\varepsilon^2}} \left[\varepsilon\left(t_1^m - t_4^m\right) + (-1)^m \Delta \sqrt{1-u^2}\left(t_2^{m+1} + t_3^{m-1}\right)\right] \Bigg\} \equiv i^{l'-l} \kappa_{l'l}^m(u',u,\varepsilon)\,. \quad (37)$$

The BTRP symmetry of the order parameter $\Delta(\hat{\mathbf{k}})$ implies that Andreev scattering involves transitions between states with m and $m \pm 1$. This mixing of channels is clarified by resolving the LDOS in the orbital angular momentum index m. Here it is worth noting that the sum over m in Eq. (34), while formally extending to $\pm\infty$, is in practice restricted to $|m| \leqslant l_{\max} \approx k_f R \approx 12$ [see Fig. 2]. Thus we resolve the LDOS as

$$N(\mathbf{r},E) = \sum_{m=-l_{\max}}^{l_{\max}} N_m(\mathbf{r},E)\,, \quad (38)$$

$$N_m(\mathbf{r},E) = \frac{1}{2l_{\max}+1} N_0(E) + \delta N_m(\mathbf{r},E)\,. \quad (39)$$

Equation (36) contains exponential factors varying on the coherence length scale, as well as fast oscillations, encoded in the spherical Bessel functions, varying on the scale of the Fermi wavelength. In Figs. 3 and 4, we averaged $\delta N_m(\mathbf{r},E)$ over a Fermi wavelength,

$$\delta N_m^{\rm qc}(\mathbf{r},E) = \frac{1}{\lambda_f} \int_{r-\lambda_f/2}^{r+\lambda_f/2} \delta N_m(\mathbf{r},E)\,, \quad (40)$$

to eliminate the atomic scale oscillations.

In Fig. 4, we plot the angular-momentum-resolved LDOS, $N_m(\mathbf{r},E)$, as a function of energy. Note that the bound states appear in neighboring pairs of m channels, and that, except for the two states with $m = 0$, the bound states for $E \geqslant 0$ ($E \leqslant 0$) occur only for channels with $m > 0$ ($m < 0$), the key feature of a Weyl spectrum of chiral fermions.

D. Bubble edge currents

The spectrum of chiral fermions bound to the electron bubble in ^{3}He-A is responsible for the ground state current circulating the bubble, the mesoscopic realization of ground-state edge currents on a macroscopic boundary of a superfluid ^{3}He-A film. The current circulating an electron bubble is calculated from the Fermi distribution and the full retarded and advanced Green's functions, $\widehat{\mathscr{G}}_{\rm S}^{\rm R,A}(\mathbf{r}',\mathbf{r};E)$, based on Eqs. (33), (16), (24), and (25)–(28),

$$\mathbf{j}(\mathbf{r}) = \frac{\hbar}{4} \int \frac{dE}{2\pi} \left(f(E) - \frac{1}{2}\right) \times (\boldsymbol{\nabla}_{\mathbf{r}'} - \boldsymbol{\nabla}_{\mathbf{r}}) {\rm Tr} \left[\widehat{\mathscr{G}}_{\rm S}^{\rm R}(\mathbf{r}',\mathbf{r};E) - \widehat{\mathscr{G}}_{\rm S}^{\rm A}(\mathbf{r}',\mathbf{r};E)\right]_{\mathbf{r}=\mathbf{r}'}. \quad (41)$$

The current circulating the electron bubble comes from the t-matrix term in Eq. (33) [44]. To calculate the current it is more efficient to recast Eq. (41) in terms of the Matsubara Green's function,

$$\mathbf{j}(\mathbf{r}) = \frac{\hbar}{4i} k_{\rm B} T \sum_{n=-\infty}^{\infty} [(\boldsymbol{\nabla}_{\mathbf{r}'} - \boldsymbol{\nabla}_{\mathbf{r}}) {\rm Tr}\, \widehat{\mathscr{G}}^{\rm M}(\mathbf{r}',\mathbf{r};\varepsilon_n)]_{\mathbf{r}=\mathbf{r}'}, \quad (42)$$

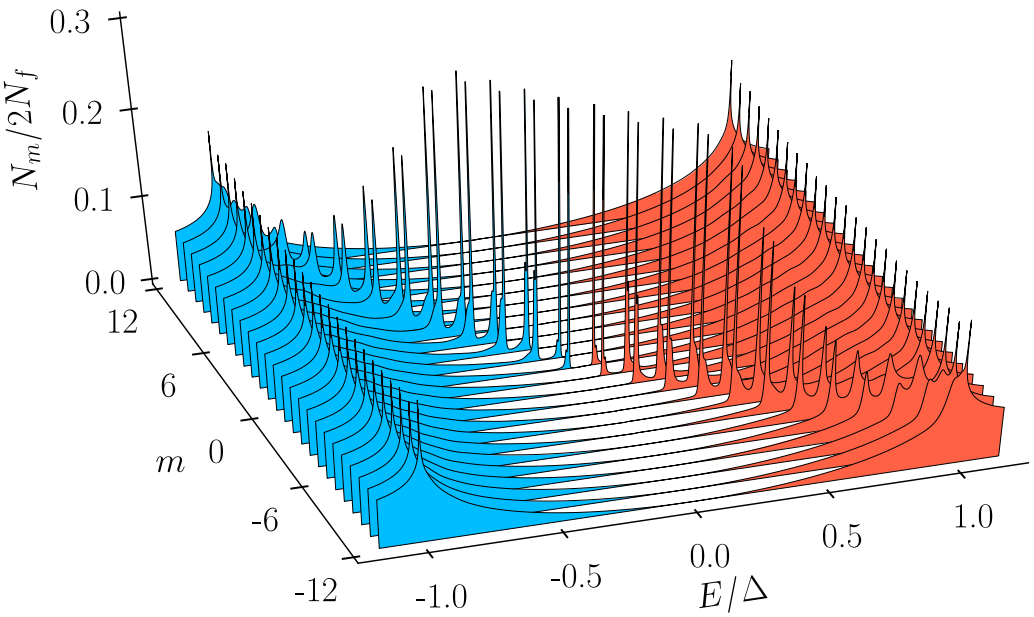

FIG. 4. The LDOS resolved into orbital angular momentum components labeled by m as defined by Eq. (39). $N_m(\mathbf{r},E)$ represents a discrete spectrum of Weyl fermions bound to the electron bubble, plus hybridization with the nodal quasiparticles. Note the double degeneracy of each subgap energy level.

where $\varepsilon_n = (2n+1)\pi k_B T$ are Matsubara frequencies, and the Matsubara Green's function is related to the retarded and advanced Green's functions by analytic continuation [45],

$$\mathscr{G}_S^{R(A)}(\mathbf{r}',\mathbf{r},E) = \mathscr{G}_S^{M}(\mathbf{r}',\mathbf{r},\varepsilon_n)\big|_{i\varepsilon_n \to E \pm i0}, \quad \text{for } \varepsilon_n \gtrless 0\,. \tag{43}$$

After Fourier-transforming Eq. (42), we obtain

$$\mathbf{j}(\mathbf{r}) = \frac{\hbar}{4} k_B T \sum_{n=-\infty}^{\infty} \left[\sum_{\mathbf{k},\mathbf{k}'} (\mathbf{k}'+\mathbf{k})\, e^{i(\mathbf{k}'-\mathbf{k})\cdot\mathbf{r}}\, \mathrm{Tr}\, \widehat{\mathscr{G}}^{M}(\mathbf{k}',\mathbf{k};\varepsilon_n) \right]. \tag{44}$$

We calculate the current from the propagator, $\widehat{\mathscr{G}}_S^{M}(\mathbf{k}',\mathbf{k};\varepsilon_n)$, by analytic continuation of the t matrix, $\widehat{T}_S^{M}(\mathbf{r}',\mathbf{r};\varepsilon_n)$, which satisfies the system of Eqs. (25)–(28), with $\varepsilon \to i\varepsilon_n$. The real valuedness of the current is ensured by the symmetry of the Nambu-Matsubara Green's function,

$$\widehat{\mathscr{G}}_S^{M}(\mathbf{k},\mathbf{k}',-\varepsilon_n) = \left[\widehat{\mathscr{G}}_S^{M}(\mathbf{k},\mathbf{k}',\varepsilon_n)\right]^{\dagger}, \tag{45}$$

which also allows us to express the result for the current as a sum over $\varepsilon_n > 0$. The current is purely azimuthal, $\mathbf{j}(r,\vartheta,\phi) = j_\phi(r,\vartheta)\mathbf{e}_\phi$ (see Appendix C), with $j_\phi(r,\vartheta)$ given by

$$j_\phi(r,\vartheta) = -8\pi^3 v_f N_f k_B T \sum_{n=0}^{\infty} \sum_{m=-\infty}^{\infty} \sum_{l'=|m-1|}^{\infty} \sum_{l=|m|}^{\infty} J_{l'l}^{m}\, \Theta_{l'}^{m-1}(\cos\vartheta)\Theta_l^m(\cos\vartheta), \tag{46}$$

$$J_{l'l}^{m} \equiv \mathrm{Im}[i^{l'-l}] \int_{-1}^{1} du' \int_{-1}^{1} du \sqrt{1-u'^2}\, \Theta_{l'}^{m-1}(u')\, e^{-\sqrt{\Delta^2(1-u'^2)+\varepsilon_n^2}\frac{r}{\hbar v_f}}\, \Theta_l^m(u)\, e^{-\sqrt{\Delta^2(1-u^2)+\varepsilon_n^2}\frac{r}{\hbar v_f}}\, \mathrm{Re}\big[\kappa_{l'l}^{m}(u',u,i\varepsilon_n)\big], \tag{47}$$

where the functions $\kappa_{l'l}^{m}(u',u,i\varepsilon_n)$ are analytically continued to the Matsubara energies, $\varepsilon \to i\varepsilon_n$.

The current circulating the electron bubble is shown in Fig. 5 for angular positions on a sphere of radius $r = 30\,k_f^{-1} \approx 3.82$ nm, i.e. in the near vicinity of the electron bubble with hard sphere radius $R = 11.17\,k_f^{-1} \approx 1.42$ nm. Note that the axial current flow is opposite to the chiralty of the ground state Cooper pairs for all polar angles, and the current vanishes in the direction of the chiral axis, i.e. along the nodal points of the order parameter. The direction of the current flow about the bubble agrees with our expectation based on the direction of the edge current for a macroscopic hole, i.e. for a locally translational invariant boundary, as illustrated in Fig. 1.

The current density varies with radial distance from the edge of the electron bubble as shown in Fig. 6. Note that the current is large on mesoscopic length scales, $R < r \ll \xi_0$, and decays very rapidly for $k_f r \gtrsim 15$. Quantum oscillations on the scale of the Fermi wavelength are evident at short distances. For $r \gtrsim \xi_0$, the current density is small and continues to decay exponentially on the scale of the coherence length as shown in the inset of Fig. 6.

The confinement of the current near the edge of the bubble endows the electron bubble with an angular momentum obtained by integrating the angular momentum density from the circulating edge current, $\mathbf{L} = \int d^3r\, \mathbf{r}\times\mathbf{j}(\mathbf{r}) = L_z\,\mathbf{e}_z$,

$$L_z = 2\pi \int_R^{\infty} r^2 dr \int_{-1}^{+1} d(\cos\vartheta)\,(r\sin\vartheta)\, j_\phi(r,\vartheta)\,, \tag{48}$$

where the lower limit is set by the vanishing of j_ϕ for $r \leqslant R$.

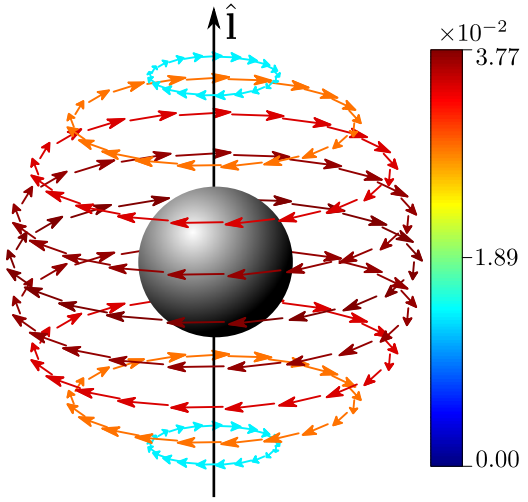

FIG. 5. Current density $\mathbf{j}(\mathbf{r})$ in units of $N_f v_f k_B T_c$ calculated at distance $k_F r = 30.0$ from the bubble center. We used the hard sphere model with $k_F R = 11.17$, shown in gray. The chiral axis $\hat{\mathbf{l}}$ determines the direction of Cooper pair angular momentum. The temperature is taken as $T = 0.5T_c$.

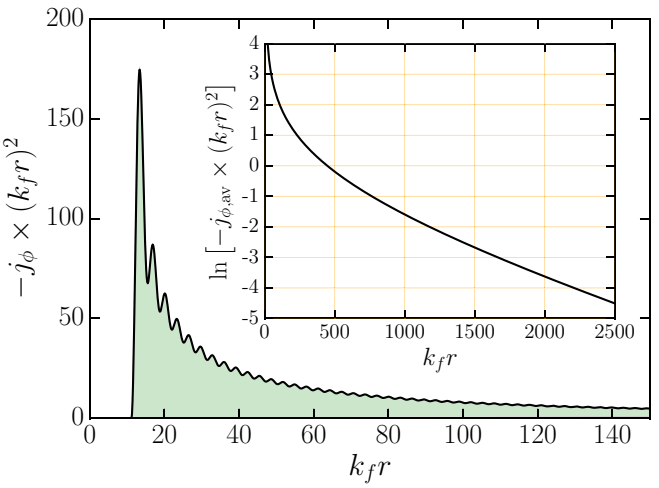

FIG. 6. Radial dependence of the current density $j_\phi(r,\vartheta)$ for $\vartheta = \pi/2$, in units of $v_f N_f k_B T_c$, calculated for the electron bubble with hard sphere radius of $k_f R = 11.17$ and temperature $T = 0.5T_c$. The current develops sharply from the bubble radius, then decays rapidly for $r > R$. Quantum oscillations on the Fermi-wave-length scale are evident at short distances. (Inset) The current decays exponentially, $j_{\phi,\mathrm{av}} \sim -e^{-r/\xi_0}/(k_f r)^2$, at distances greater than the coherence length, $\xi_0 = 608.7\,k_f^{-1}$; $j_{\phi,\mathrm{av}}$ is the quasiclassical envelope obtained by averaging $j_\phi(r)$ over a Fermi wavelength as in Eq. (40).

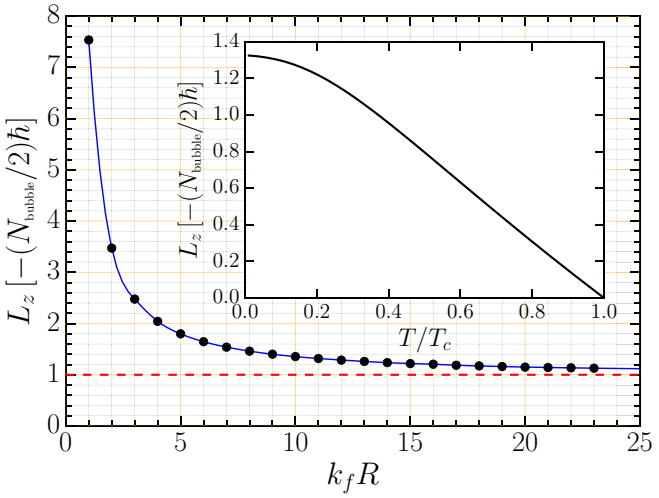

FIG. 7. Angular momentum of hard sphere "bubbles" embedded in ^{3}He-A as a function of hard sphere radius, k_fR. For an electron bubble, $k_fR = 11.17$. In the macroscopic limit, $R \gg \xi_0$ (red dashed line), L_z scales to $L_z^\infty = -(N_{\rm bubble}/2)\,\hbar$. (Inset) Temperature dependence of L_z for the electron bubble.

Recalling our result for the angular momentum generated by edge currents circulating a macroscopic hole of radius $R \gg \xi_0$ in a thin ^{3}He-A film, we express the angular momentum of the electron bubble edge currents in similar units, i.e.

$$L_z = -\mathfrak{f}\left(\frac{N_{\rm bubble}}{2}\right)\hbar\,, \tag{49}$$

$$N_{\rm bubble} = \frac{4}{9\pi}(k_fR)^3 \approx 197\,, \tag{50}$$

where $N_{\rm bubble}$ is the number of ^{3}He atoms excluded from the electron bubble. The negative sign reflects the fact that the angular momentum of the chiral currents is opposite to the chirality of the Cooper pairs. Numerical integration of Eq. (48) gives $\mathfrak{f} = 1.3$, remarkably close to the prediction based on the volume of a macroscopic hole ($R \gg \xi_0$) in a ^{3}He-A film, even though the electron bubble is in the limit $R \ll \xi_0$. Indeed, the angular momentum calculated for mesoscopic hard sphere bubbles, scaled in units of $-(N_{\rm bubble}/2)\hbar$, is shown in Fig. 7 to rapidly approach the macroscopic scaling result for $k_fR \gg 1$. Already at $k_fR = 25$, which corresponds to $R/\xi_0 \approx 0.04$, the deviation from the macroscopic scaling result is only ≈7%. The inset of Fig. 7 shows the temperature dependence of L_z for the electron bubble, scaling as $|\Delta(T)|^2 \sim |T - T_c|$ in the Ginzburg-Landau (GL) limit [46].

IV. ELECTRON MOBILITY IN ^{3}He-A

Application of a dc electric field accelerates the electron bubble to a terminal velocity $\mathbf{v} = \overleftrightarrow{\mu}\cdot\mathbf{E}$, where the mobility, $\overleftrightarrow{\mu}$, is determined by forces acting on the moving electron bubble. At finite temperature, the mobility is limited by the "wind" of thermal quasiparticles scattering off the moving electron bubble. In the normal phase of ^{3}He, the scattering rate is sufficiently large that recoil of the ion is suppressed, implying elastic scattering and a normal-state mobility that is temperature independent [34,47]. Below T_c, the opening of a gap in the excitation spectrum leads to a rapid increase in the mobility [48]. Experimentally, the mobility increases faster than expected based just on the reduction in the number of thermal quasiparticles. Baym *et al.* [38] showed that in the superfluid B phase the transport cross section is also reduced by resonant forward scattering of Bogoliubov quasiparticles off the electron bubble. Their theory provides quantitative agreement with measurements of the mobility in ^{3}He-B in the temperature regime near T_c [49].

For the chiral A phase, these two basic features also operate. However, superfluid ^{3}He-A has an anisotropic excitation gap that vanishes for momenta $\mathbf{k}||\pm\hat{\mathbf{l}}$ and is maximal for momenta $\mathbf{k}\perp\hat{\mathbf{l}}$. Thus an electron bubble will experience a stronger drag force for $\mathbf{v}||\pm\hat{\mathbf{l}}$ compared to $\mathbf{v}\perp\hat{\mathbf{l}}$, i.e. $\mu_{||} < \mu_\perp$. Indeed the anisotropy of the negative ion mobility was calculated by extending the scattering theory for the B phase by Baym *et al.* [38] to scattering by an ion in ^{3}He-A [22,50], and measurements of the mobility anisotropy, $\mu_\perp - \mu_{||}$, were made via pulse-shape, time-of-flight experiments on vortex textures of superfluid ^{3}He-A [51]. Note that the drag force on the electron bubble is insensitive to the direction of the chiral axis, i.e. the drag force for $+\mathbf{E}||\hat{\mathbf{l}}$ and $-\mathbf{E}||\hat{\mathbf{l}}$ are the same.

The chiral axis is a reflection of broken time-reversal symmetry (T) and broken mirror symmetry (Π) in a plane containing the chiral axis $\hat{\mathbf{l}}$. The generalization of the mobility for the isotropic B phase to ^{3}He-A with chiral axis $\hat{\mathbf{l}}||\hat{\mathbf{z}}$ is a mobility tensor, μ_{ij} with $i,j \in \{x,y.z\}$; thus, $v_i = \mu_{ij}E_j$, where the components are all real. Uniaxial rotation symmetry restricts the elements of the mobility tensor to $\mu_{xx} = \mu_{yy} \equiv \mu_\perp$, $\mu_{zz} \equiv \mu_{||}$, and $\mu_{xy} = -\mu_{yx}$; all other components vanish. Thus the electron mobility tensor for ^{3}He-A has the form

$$\mu_{ij} = \mu_\perp(\delta_{ij} - \hat{\mathbf{l}}_i\hat{\mathbf{l}}_j) + \mu_{||}\hat{\mathbf{l}}_i\hat{\mathbf{l}}_j + \mu_{xy}\varepsilon_{ijk}\hat{\mathbf{l}}_k\,. \tag{51}$$

The off-diagonal component, μ_{xy}, is allowed by axial rotation symmetry and chiral symmetry, $\mathrm{C} = \mathrm{T}\times\Pi$, but vanishes if the ground state is separately invariant under mirror symmetry, Π, in a plane containing the chiral axis $\hat{\mathbf{l}}$. This would be the case for a Planar phase of ^{3}He, which is degenerate in weak-coupling theory with the A phase, has the same anisotropic excitation gap, and thus, is indistinguishable from ^{3}He-A in terms of $\mu_{||}$ and $\mu_\perp$. What distinguishes the A phase is that neither T nor Π are symmetries. The breaking of both T and Π allows for $\mu_{xy} \neq 0$, and thus transverse motion of the electron bubble for $\mathbf{E}\perp\hat{\mathbf{l}}$, i.e. an anomalous Hall current of electron bubbles given by

$$\mathbf{v}_{\rm AH} = \mu_{xy}\,\mathbf{E}\times\hat{\mathbf{l}}\,. \tag{52}$$

More generally, for any field orientation, the steady state ion velocity is given by

$$\mathbf{v} = \mu_\perp\hat{\mathbf{l}}\times(\mathbf{E}\times\hat{\mathbf{l}}) + \mu_{||}(\hat{\mathbf{l}}\cdot\mathbf{E})\,\hat{\mathbf{l}} + \mu_{xy}\mathbf{E}\times\hat{\mathbf{l}}\,. \tag{53}$$

This steady-state result for the velocity arises from the balance between the Coulomb force, $\mathbf{F}_\mathbf{E} = e\mathbf{E}$, and the quasiparticle force, $\mathbf{F}_{\rm QP} = -\overleftrightarrow{\eta}\cdot\mathbf{v}$, where $\overleftrightarrow{\eta}$ is the generalized Stokes tensor for an anisotropic fluid. The latter determines the inverse of the mobility tensor, $\overleftrightarrow{\eta} = e\overleftrightarrow{\mu}^{-1}$, and has the same structure as the mobility tensor, $\eta_{ij} = \eta_\perp(\delta_{ij} - \hat{\mathbf{l}}_i\hat{\mathbf{l}}_j) + \eta_{||}\hat{\mathbf{l}}_i\hat{\mathbf{l}}_j + \eta_{xy}\varepsilon_{ijk}\hat{\mathbf{l}}_k$. Theoretically, we determine the force on a moving ion, i.e. the Stokes tensor. The components of the

mobility are then given by the inversion formulas,

$$\mu_\perp = e\frac{\eta_\perp}{\eta_\perp^2+\eta_{xy}^2},\quad \mu_{xy} = e\frac{-\eta_{xy}}{\eta_\perp^2+\eta_{xy}^2},\quad \mu_{||} = e\frac{1}{\eta_{||}}. \tag{54}$$

A. Quasiparticles forces on an electron bubble

We formulate the microscopic theory for the forces acting on a moving electron bubble due to scattering by thermal quasiparticles in the chiral A phase of ^{3}He. The key assumptions are (i) that the velocity of the electron bubble is sufficiently low that the resulting Stokes tensor, η_{ij}, is independent of the electron velocity, (ii) the recoil energy of the ion is sufficiently low, $\Delta_{\rm rec} \ll k_BT$, that it is a good approximation to consider quasiparticle-ion scattering in the elastic limit, (iii) the ground state is described by the ESP chiral A-phase order parameter in Eq. (11), and (iv) the only input parameters to the theory are the normal state scattering phase shifts constrained by the normal state mobility [Eq. (9) and Fig. 2].

Our analysis is close to that of Baym *et al.* for the ion mobility in ^{3}He-B [38,52], except that we incorporate broken time-reversal and mirror symmetries of the chiral ground state into the theory of the transport cross section for scattering of Bogoliubov quasiparticles off the electron bubble embedded in ^{3}He-A. Earlier theoretical analyses of the electron mobility in ^{3}He-A included the ansisotropy of the excitation spectrum, but imposed mirror symmetry in the formulation of the scattering of Bogoliubov quasiparticles off the ion embedded in ^{3}He-A [22–24]. See Appendix A for our critique of earlier work.

In what follows, we derive results for the scattering cross section and forces on a negative ion moving in superfluid ^{3}He-A driven by a static electric field. We start from the equation of motion for the momentum of the ion,

$$\frac{d\mathbf{P}}{dt} = -\sum_{\mathbf{k},\mathbf{k}'}\hbar(\mathbf{k}'-\mathbf{k})(1-f_{\mathbf{k}'})f_{\mathbf{k}}\,\Gamma_{\mathbf{v}}(\mathbf{k}',\mathbf{k}), \tag{55}$$

where $\hbar(\mathbf{k}-\mathbf{k}')$ is the momentum transferred to the ion by scattering of a quasiparticle from $\mathbf{k}\to\mathbf{k}'$, $f_{\mathbf{k}}$ is the probability that the incident state $\mathbf{k}$ is occupied, $(1-f_{\mathbf{k}'})$ is the probability that the final state $\mathbf{k}'$ is unoccupied, and $\Gamma_{\mathbf{v}}(\mathbf{k}',\mathbf{k})$ is the transition rate of scattering of quasiparticles by the ion moving with velocity $\mathbf{v}$. In the low-velocity limit, the forces are linear in $\mathbf{v}$. The generalization of the theory presented here to higher velocities when inelastic scattering and nonlinear velocity dependence becomes important is outside the scope of this report, but can be formulated as a generalization of the theory of Josephson and Lekner for the dynamics of electrons in normal ^{3}He [34].

In the low-velocity limit, the motion of an ion does not substantially perturb the initial and final quasiparticle distribution functions, i.e. the ion moves through a Fermi-Dirac distribution of quasiparticles described by temperature T, $f_{\mathbf{k}} = f(E_{\mathbf{k}}) \equiv [1+\exp(E_{\mathbf{k}}/k_BT)]^{-1}$, where the bulk ^{3}He-$A$ excitation energy is $E_{\mathbf{k}} = \sqrt{\xi_{\mathbf{k}}^2+|\Delta(\mathbf{k})|^2}$.

To linearize Eq. (55) in the ion velocity, we follow Baym *et al.* [53] and observe that if the distribution of quasiparticles were in thermal equilibrium and co-moving with the electron bubble, then the initial and final state distribution functions would be Doppler-shifted Fermi-Dirac distributions,

$$\bar{f}_{\mathbf{k}} = f(E_{\mathbf{k}} - \hbar\mathbf{k}\cdot\mathbf{v}). \tag{56}$$

In this case, the net momentum transfer is zero. We then subtract zero from Eq. (55) to obtain

$$\frac{d\mathbf{P}}{dt} = -\sum_{\mathbf{k},\mathbf{k}'}\hbar(\mathbf{k}'-\mathbf{k})[f_{\mathbf{k}}(1-f_{\mathbf{k}'}) - \bar{f}_{\mathbf{k}}(1-\bar{f}_{\mathbf{k}'})]\Gamma_{\mathbf{v}}(\mathbf{k}',\mathbf{k}). \tag{57}$$

The momentum transfer to the ion is a sum over all incident and final state momenta. For every transition, $\mathbf{k}\to\mathbf{k}'$, there is a mirror scattering event, $\mathbf{k}'\to\mathbf{k}$, that contributes to the net transfer of momentum to the ion. In order to isolate the scattering events responsible for the anomalous Hall mobility, it is convenient to symmetrize the right-hand side of Eq. (57) and express the momentum transfer rate in terms of pairs of transition rates related by mirror symmetry,

$$\begin{aligned}\frac{d\mathbf{P}}{dt} = -\frac{1}{2}\sum_{\mathbf{k},\mathbf{k}'}\hbar(\mathbf{k}'-\mathbf{k})\{&[f_{\mathbf{k}}(1-f_{\mathbf{k}'}) - \bar{f}_{\mathbf{k}}(1-\bar{f}_{\mathbf{k}'})]\Gamma_{\mathbf{v}}(\mathbf{k}',\mathbf{k})\\ &- [f_{\mathbf{k}'}(1-f_{\mathbf{k}}) - \bar{f}_{\mathbf{k}'}(1-\bar{f}_{\mathbf{k}})]\Gamma_{\mathbf{v}}(\mathbf{k},\mathbf{k}')\}.\end{aligned} \tag{58}$$

A key point is that the phase space factors for allowed transitions—the terms in square brackets—are already linear in the ion velocity $\mathbf{v}$. Thus we evaluate the transition rate $\Gamma_{\mathbf{v}}$ in the static limit, $\Gamma_{\mathbf{v}}(\mathbf{k}',\mathbf{k})\to\Gamma(\mathbf{k}',\mathbf{k})$, with the latter given by Fermi's golden rule,

$$\Gamma(\mathbf{k}',\mathbf{k}) = \frac{2\pi}{\hbar}W(\mathbf{k}',\mathbf{k})\delta(E_{\mathbf{k}'}-E_{\mathbf{k}}), \tag{59}$$

where $W(\mathbf{k}',\mathbf{k})$ is the transition rate for Bogoliubov quasiparticles, defined by the Bogoliubov-Nambu spinors in Eqs. (12) and (13), scattering off the electron bubble,

$$\begin{aligned}W(\mathbf{k}',\mathbf{k}) = \frac{1}{2}\sum_{\sigma,\sigma'=\uparrow,\downarrow}\{&|\langle\,\Psi_{1,\mathbf{k}'\sigma'}\,|\widehat{T}_S|\,\Psi_{1,\mathbf{k}\sigma}\,\rangle|^2\\ &+|\langle\,\Psi_{1,\mathbf{k}'\sigma'}\,|\widehat{T}_S|\,\Psi_{2,\mathbf{k}\sigma}\,\rangle|^2\\ &+|\langle\,\Psi_{2,\mathbf{k}'\sigma'}\,|\widehat{T}_S|\,\Psi_{1,\mathbf{k}\sigma}\,\rangle|^2\\ &+|\langle\,\Psi_{2,\mathbf{k}'\sigma'}\,|\widehat{T}_S|\,\Psi_{2,\mathbf{k}\sigma}\,\rangle|^2\}_{E_{\mathbf{k}'}=E_{\mathbf{k}}}.\end{aligned} \tag{60}$$

The result for the scattering rate for Bogoliubov quasiparticles is a sum over the possible elastic scattering events between Bogoliubov particlelike (1) and holelike (2) branches of the excitation spectrum: $1\to1$, $2\to1$, $1\to2$, and $2\to2$. Expanding the Doppler-shifted Fermi functions in Eq. (58) to linear order in $\mathbf{v}$ yields

$$\begin{aligned}\frac{d\mathbf{P}}{dt} = -\frac{3}{2}\hbar k_f n_3 k_f^{-2}&\left(\frac{m^*}{2\pi\hbar^2}\right)^2\int d\Omega_{\mathbf{k}}\int\frac{d\Omega_{\mathbf{k}'}}{4\pi}\int_{|\Delta(\mathbf{k})|}^{\infty}dE\int_{|\Delta(\mathbf{k}')|}^{\infty}dE'\,\delta(E-E')\frac{EE'}{\sqrt{E^2-|\Delta(\mathbf{k})|^2}\sqrt{E'^2-|\Delta(\mathbf{k}')|^2}}\left(-\frac{\partial f}{\partial E}\right)\\ &\times(\mathbf{k}'-\mathbf{k})\{W(\mathbf{k}',\mathbf{k})\,[\mathbf{k}'f-\mathbf{k}(1-f)] - W(\mathbf{k},\mathbf{k}')\,[\mathbf{k}f-\mathbf{k}'(1-f)]\}\cdot\mathbf{v},\end{aligned} \tag{61}$$

where $f = [\exp(E/k_BT)+1]^{-1}$ and we used the fact that the momenta are restricted to, $|k-k_f| \ll k_f$, and energies are confined to a shell near the Fermi surface, $|\xi_{\mathbf{k}}| = v_f|(k-k_f| \ll E_f$. We changed energy integration variables from $d\xi_{\mathbf{k}} \to dE_{\mathbf{k}}$ with $\xi_{\mathbf{k}} = \pm\sqrt{E_{\mathbf{k}}^2 - |\Delta(\hat{\mathbf{k}})|^2}$, where $\xi_k > 0$ and $\xi_k < 0$ correspond to particlelike and holelike excitations, respectively. In Eq. (61) and hereafter, the momenta are evaluated on the Fermi surface: $\mathbf{k} = k_f\hat{\mathbf{k}}$ and $\mathbf{k}' = k_f\hat{\mathbf{k}}'$, and $W(\mathbf{k}',\mathbf{k}) = W(\hat{\mathbf{k}}',\hat{\mathbf{k}};E)$.

B. Microscopic reversibility and mirror symmetry

If the ground state in which the ion is embedded were time-reversal and mirror symmetric we could use the "microscopic reversibility" condition, $W(\mathbf{k}',\mathbf{k}) = W(\mathbf{k},\mathbf{k}')$. This is the case for the B phase of ^{3}He, which also has a rotational invariant excitation spectrum and bulk gap, $|\Delta(\hat{\mathbf{k}})| = \Delta$. Equation (61) then reduces to $d\mathbf{P}/dt = -\eta\,\mathbf{v}$, with the Stokes drag coefficient, and thus the inverse mobility, given by

$$\eta = \frac{e}{\mu} = n_3\, p_f \int_\Delta^\infty dE\, \sigma^{\rm tr}(E)\left(-2\frac{\partial f}{\partial E}\right) \tag{62}$$

where the energy resolved transport cross section is

$$\sigma_{\rm tr}(E) = \left|\frac{m^*}{2\pi\hbar^2}\frac{d\xi}{dE}\right|^2 \int d\Omega_{\mathbf{k}'} W_{\rm B}(\hat{\mathbf{k}}'\cdot\hat{\mathbf{k}};E)\,(1-\hat{\mathbf{k}}'\cdot\hat{\mathbf{k}}), \tag{63}$$

in agreement with the result for the mobility obtained for ^{3}He-B by Baym *et al.* [38]. In the limit $\Delta \to 0$, this result reduces to the mobility of normal ^{3}He given by Eq. (3).

The theory for the mobility of ^{3}He-B was extended by Salomaa *et al.* to calculate the mobility tensor ^{3}He-A [22]. These authors included the anisotropy of the excitation gap, $|\Delta(\hat{\mathbf{k}})|$. However, they implicitly assumed mirror symmetry by imposing the microscopic reversibility condition for mirror symmetric scattering events. Microscopic reversibility implies that the second line of Eq. (61) reduces to $\times(\mathbf{k}'-\mathbf{k})\,W(\mathbf{k}',\mathbf{k})\,(\mathbf{k}'-\mathbf{k})\cdot\mathbf{v}$. The resulting momentum transfer to the ion by quasiparticle scattering is then given by a *symmetric* Stokes tensor, and thus there is no transverse force on the moving ion. Indeed, in Ref. [22], the uniaxial anisotropy of the mobility tensor was calculated, but no anomalous Hall term was reported.

Existence of a transverse force acting on an electron bubble moving in ^{3}He-A was argued on physical grounds by Salmelin *et al.* [23] based on the prediction of currents circulating an impurity in superfluid ^{3}He-A [7], and the analogy with the Magnus effect arising from the hydrodynamic lift force on a rotating sphere moving through a fluid [54]. The authors dubbed the transverse force on a moving ion in ^{3}He-A an "intrinsic Magnus effect," and they focused their discussion on the limit of a small object such as an electron bubble with radius $R \ll \xi_0$, small in comparison to the size of the Cooper pairs in ^{3}He-A.

Although the basic picture motivating the existence of a transverse force on electron bubbles moving through a chiral superfluid is sound, the microscopic theory outlined in Ref. [23] and published in detail by Salmelin and Salomaa in Ref. [24], is fundamentally flawed. These authors impose mirror symmetry in their calculation of the scattering amplitude for momentum transfer from the distribution of quasiparticles to the moving ion by adopting the microscopic reversibility condition $W(\mathbf{k}',\mathbf{k}) = W(\mathbf{k},\mathbf{k}')$. This equality guarantees, within scattering theory, that there is no transverse force on the electron bubble. As a consequence the theoretical results and prediction for the transverse Hall mobility in Refs. [23,24] are spurious. We include a more detailed critique of this work in Appendix A. In the following section, we show that it is precisely the asymmetry in scattering rates for $\mathbf{k} \to \mathbf{k}'$ and its mirror symmetric partner, $\mathbf{k}' \to \mathbf{k}$, that is the origin of the transverse force acting on a moving electron bubble.

C. Scattering cross sections and the mobility tensor

A central feature of Eq. (61) is that the rates $W(\mathbf{k}',\mathbf{k})$ and $W(\mathbf{k},\mathbf{k}')$ for mirror symmetric scattering events are *not equal* for chiral ground states like that of superfluid ^{3}He-A. To highlight the importance of this fact, we separate $W(\mathbf{k}',\mathbf{k})$ into its mirror symmetric (W^+) and antisymmetric (W^-) parts,

$$W(\mathbf{k}',\mathbf{k}) = W^{(+)}(\mathbf{k}',\mathbf{k}) + W^{(-)}(\mathbf{k}',\mathbf{k}), \tag{64}$$

with $W^{(\pm)}(\mathbf{k}',\mathbf{k}) = \pm W^{(\pm)}(\mathbf{k},\mathbf{k}')$. Equation (61) for the force on the moving ion is linear in the ion velocity, $d\mathbf{P}/dt = -\overleftrightarrow{\eta}\cdot\mathbf{v}$, and can be expressed in terms of the components of the Stokes tensor

$$\eta_{ij} = n_3 p_f \int_0^\infty dE\left(-2\frac{\partial f}{\partial E}\right)\sigma_{ij}(E), \quad i,j \in \{x,y,z\}, \tag{65}$$

where $\sigma_{ij}(E) = \sigma_{ij}^{(+)}(E) + \sigma_{ij}^{(-)}(E)$ is the energy-resolved transport cross section separated into symmetric (+) and antisymmetric (−) tensor components, $\sigma_{ij}^{(\pm)}(E)$, which are given by Fermi surface averages over the differential cross section,

$$\frac{d\sigma}{d\Omega_{\mathbf{k}'}}(\hat{\mathbf{k}}',\hat{\mathbf{k}};E) = \left(\frac{m^*}{2\pi\hbar^2}\right)^2 \frac{E}{\sqrt{E^2-|\Delta(\hat{\mathbf{k}}')|^2}}\, W(\mathbf{k}',\mathbf{k}) \frac{E}{\sqrt{E^2-|\Delta(\hat{\mathbf{k}})|^2}}, \tag{66}$$

$$\sigma_{ij}^{(+)}(E) = \frac{3}{4}\int_{E\geqslant|\Delta(\hat{\mathbf{k}}')|} d\Omega_{\mathbf{k}'} \int_{E\geqslant|\Delta(\hat{\mathbf{k}})|} \frac{d\Omega_{\mathbf{k}}}{4\pi}[(\hat{\mathbf{k}}'_i-\hat{\mathbf{k}}_i)(\hat{\mathbf{k}}'_j-\hat{\mathbf{k}}_j)]\frac{d\sigma}{d\Omega_{\mathbf{k}'}}(\hat{\mathbf{k}}',\hat{\mathbf{k}};E), \tag{67}$$

$$\sigma_{ij}^{(-)}(E) = \frac{3}{4}\int_{E\geqslant|\Delta(\hat{\mathbf{k}}')|} d\Omega_{\mathbf{k}'} \int_{E\geqslant|\Delta(\hat{\mathbf{k}})|} \frac{d\Omega_{\mathbf{k}}}{4\pi}[\varepsilon_{ijk}(\hat{\mathbf{k}}'\times\hat{\mathbf{k}})_k]\frac{d\sigma}{d\Omega_{\mathbf{k}'}}(\hat{\mathbf{k}}',\hat{\mathbf{k}};E)\left[f(E)-\frac{1}{2}\right]. \tag{68}$$

Equations (65) and (68) combined with Eqs. (60) and (25)–(28) to compute the scattering rate $W(\mathbf{k}',\mathbf{k})$, are the central results for the forces on a moving electron bubble. The Stokes tensor determines both the drag forces, $\propto\eta_{\perp,||}$, and the transverse force, $\propto\eta_{xy}$, responsible for the anomalous Hall effect on moving electron bubbles in chiral superfluid phase of ^{3}He.

Note that Eq. (67) for the symmetric part of the transport cross section is equivalent to Eqs. (7) and (8) of Ref. [24]. This is a symmetric tensor, and as is clear from the integrand of Eq. (67) *only* the symmetric part of the scattering rate, $W^{(+)}(\mathbf{k}',\mathbf{k})$, contributes to $\sigma_{ij}^{(+)}(E)$. Thus $\sigma_{ij}^{(+)}(E)$ contributes only to the diagonal components of the Stokes tensor; there is no anomalous Hall term contained in Eq. (67). The errors leading the authors of Refs. [23,24] to obtain $\sigma_{xy}^{(+)} \neq 0$ are identified and discussed in Appendix A.

The antisymmetric part of the transport cross section given by Eq. (68) is the origin of the transverse force on a moving electron bubble. This is a new result that is present because quasiparticle scattering off an electron bubble embedded in a chiral superfluid acquires a spectrum of chiral fermions bound to the electron bubble. As a result, the scattering rates for $\mathbf{k} \to \mathbf{k}'$ and the mirror-symmetric scattering event, $\mathbf{k}' \to \mathbf{k}$, are not equal. From the integrand of Eq. (68) it is clear that *only* the antisymmetric part of the scattering rate, $W^{(-)}(\mathbf{k}',\mathbf{k})$, contributes to $\sigma_{ij}^{(-)}(E)$. The antisymmetric cross section, $\sigma_{ij}^{(-)}(E)$, determines the off-diagonal components of the Stokes tensor, and thus the transverse force acting on the moving electron bubble [55]. Note that $\sigma_{ij}^{(-)}(E)$ is identically zero if the condition of microscopic reversibility is assumed to hold, i.e. $W^{(-)} \equiv 0$. Also note the distribution function, $f(E) - \frac{1}{2} = -\frac{1}{2}\tanh(E/2k_BT)$, appearing in Eq. (68) is odd under $E \to -E$. This implies that the transverse force originates from the chiral part of the spectrum, which is a reflection of branch conversion scattering between particlelike and holelike excitations by the chiral order parameter.

Lastly, for $|\Delta(\hat{\mathbf{k}})| = 0$, Eqs. (67) and (68) reduce to the normal-state transport cross section given in Eq. (8),

$$\sigma_{ij}^{(+)}(E) \to \delta_{ij}\,\sigma_{\rm N}^{\rm tr}\,, \quad \sigma_{ij}^{(-)}(E) \to 0\,, \tag{69}$$

where $\sigma_{ij}^{(-)}(E)$ vanishes because the gauge and mirror symmetries are unbroken in the normal Fermi liquid. Integration over energy in Eq. (65) gives unity and we obtain the Stokes drag, and thus the temperature independent normal-state mobility given by Eq. (3).

V. RESULTS FOR THE e$^-$ MOBILITY IN ^{3}He-*A*

Our formulation of the scattering theory was motivated in part by the reports of the RIKEN group of an anomalous Hall effect in their measurements of electron transport in superfluid ^{3}He-*A* for temperatures down to $T \approx 250\,\mu$K [8,9]. In these experiments, electrons are forced to a depth of 30 nm below the free surface of liquid ^{3}He by a perpendicular electric field. The electrons form negatively charged bubbles with an effective mass $M \approx \frac{2}{9\pi}(k_fR)^3\,m_3 \approx 100\,m_3$, where m_3 is the mass of the ^{3}He atom [47]. For ^{3}He-*A*, the chiral axis is locked normal to the free surface, $\hat{\mathbf{l}}||\hat{\mathbf{z}}$. The electron bubbles are then driven into motion by an additional electric field $\mathbf{E} = \mathscr{E}\,\mathbf{e}_x$ applied in the xy plane. A pair of split electrodes are used to measure both the longitudinal current, $v_x = \mu_{xx}\mathscr{E}$, and the Hall current, $v_y = \mu_{xy}\mathscr{E}$ [56].

The RIKEN group also compared their measurements of the anomalous Hall angle for electron bubbles in superfluid ^{3}He-*A*, with calculations based on the theoretical formulas for the longitudinal and transverse mobilities published in Ref. [24]. However, the comparison is based on a fundamentally flawed theory of the mobility tensor, particularly the anomalous Hall effect (see discussion in Appendix A). As a result, the comparison shows inconsistencies between the size of the electron bubble as determined from the normal state mobility, $k_fR = 11.17$, and the hard sphere radius that was used to account for the longitudinal mobility in the superfluid phase, $k_fR = 16$. Even with this much larger electron bubble radius, the calculated Hall ratio, η_{xy}/η_{xx}, based on the formulas of Refs. [23,24], is a factor of two to four smaller than the observed Hall effect [8].

In the following, we show that the scattering theory for the Stokes tensor for electron bubbles moving in ^{3}He-*A* presented in Secs. II–IV provides a quantitative account of the magnitude and temperature dependences of both the longitudinal mobility and the anomalous Hall effect within the hard-sphere model for the interaction of ^{3}He quasiparticles with the electron bubble. The only parameter in the theory is the hard sphere radius which we determine by fitting the transport cross section for hard-sphere scattering to the normal-state mobility to obtain $k_fR = 11.17$. The electron-quasiparticle interaction is then determined by the hard sphere scattering phase shifts in Eq. (9), and plotted in Fig. 2.

The calculations presented here for the transport cross sections and resultant components of the Stokes tensor are obtained by first solving the linear integral Eqs. (25)–(28) for the t matrix amplitudes, $t_a^m(u',u)$. We transform the integral equations to coupled algebraic equations using Gauss-Legendre quadrature rules of even order, and integrate the square-root singularities appearing in the propagators following the procedure given in Ref. [57].

A. Scattering cross sections

In Fig. 8, we show results for the differential cross section defined in Eqs. (64) and (66) for in-plane scattering, i.e. both incident, $\mathbf{k}$, and scattered, $\mathbf{k}'$, wave vectors in the xy plane. In particular, for an incoming quasiparticle with $\hat{\mathbf{k}} = \mathbf{e}_x$ ($\theta = \pi/2, \phi = 0$) the symmetric part of the angular distribution, $d\sigma^{(+)}/d\Omega_{\mathbf{k}'}$, contributing to $\sigma_{ij}^{(+)}(E)$ is shown in panel (a), and the asymmetry in the angular distribution, $d\sigma^{(-)}/d\Omega_{\mathbf{k}'}$, of the scattered excitations is shown in panel (b) as a function of the azimuthal scattering angle $\Delta\phi = \phi' - \phi$. Note that $d\sigma^{(-)}/d\Omega_{\mathbf{k}'}$ changes sign across the lines $\Delta\phi = 0$ and $\Delta\phi = \pi$, and determines the antisymmetric, transverse cross section, $\sigma_{ij}^{(-)}(E)$. The total differential cross section is shown in Fig. 8(c) in comparison with that for quasiparticle-ion scattering in the normal state. There is strong reduction in backscattering in the superfluid state compared to that in the normal state, as well as the sharp angular dependencies associated with resonant scattering from the spectrum of chiral fermions bound to the ion, evident in the angular momentum resolved density of states shown in Fig. 4. Resonant scattering of quasiparticles by the spectrum of chiral fermions bound to the electron bubble is also evident in the energy-resolved transport cross sections, $\sigma_{xy}^{(-)}(E)$ and $\sigma_{xx}^{(+)}(E)$, shown in Fig. 9 normalized by the normal state transport cross section.

One can clearly see the peak-dip structure at energies below the maximum gap Δ. These structures are due to resonant scattering from chiral fermions bound to the surface of the electron bubble. There is a resonance for each angular momentum channel m. The chiral fermions form as a result of multiple potential and Andreev scattering of quasiparticles off

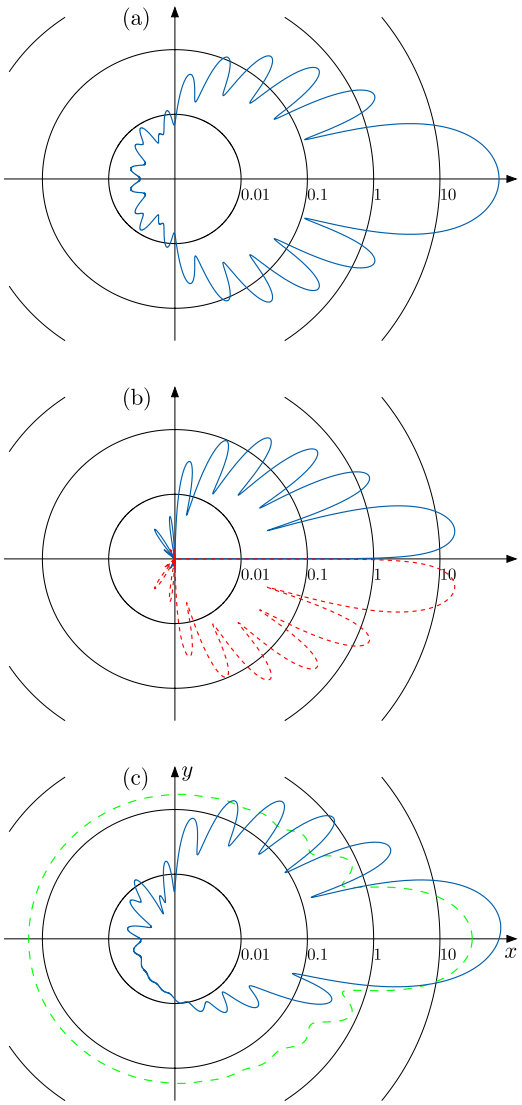

FIG. 8. Panel (a) shows a polar plot of the differential cross section, $d\sigma^{(+)}(\hat{\mathbf{k}}',\hat{\mathbf{k}};E)/d\Omega_{\mathbf{k}'}$, as a function of the in-plane scattering angle angle $\phi'-\phi$ [Eqs. (64) and (66)], with incoming and outgoing momenta lying in the xy plane, i.e. $\theta'=\theta=\pi/2$ and $\hat{\mathbf{k}}=\mathbf{e}_x$ ($\phi=0$). The contours mark the magnitudes of the differential cross sections in units of πR^2 on a logarithmic scale. The quasiparticle energy is $E=1.01\Delta$, and the ion-quasiparticle potential is a hard sphere with $k_f R=11.17$. Similarly, (b) shows the asymmetry in the angular distribution of scattered quasiparticles given by $d\sigma^{(-)}(\hat{\mathbf{k}}',\hat{\mathbf{k}};E)/d\Omega_{\mathbf{k}'}$, which changes sign continuously across the lines $\Delta\phi=0,\pi$. The sign change is indicated by the dashed red curve. (c) shows the sum of these two differential cross sections, highlighting the asymmetry in the angular distribution of scattering quasiparticles for $\mathbf{l}\|\mathbf{z}$. The angular distribution for quasiparticle-ion scattering in the normal state is shown as the dashed green line.

the electron bubble and the chiral order parameter in which it is embedded. This multiple scattering and bound state formation is encoded in the t matrix equations of Eqs. (25)–(28).

B. Forces on moving electron bubbles

The transport cross sections, $\sigma_{ij}^{(+)}(E)$ and $\sigma_{ij}^{(-)}(E)$ calculated for the hard sphere potential, are used to calculate the

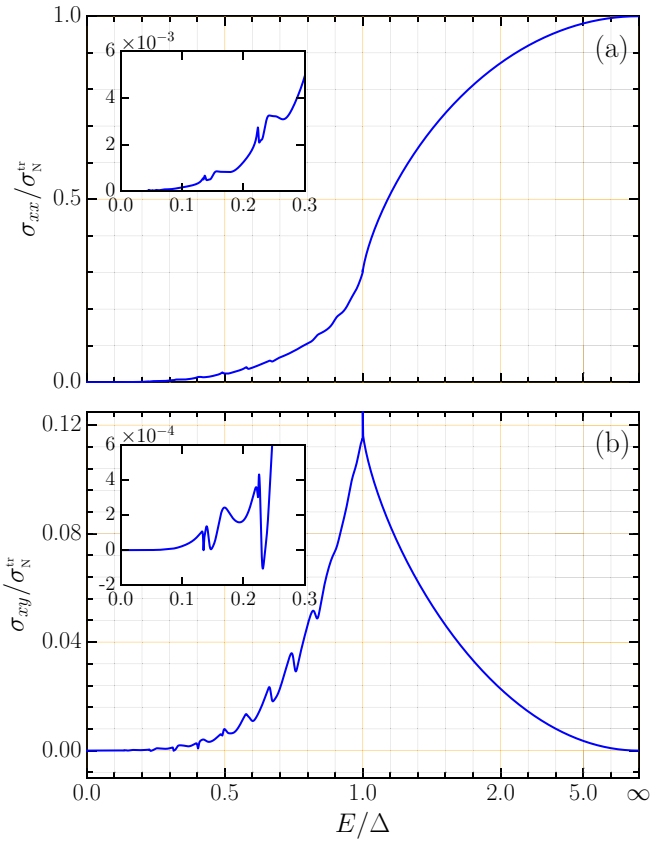

FIG. 9. The longitudinal (a) and transverse (b) transport cross sections as a function of energy for $T=0.5T_c$. The peak-dip structure at energies below the maximum gap Δ are resonances originating from scattering of quasiparticles by chiral fermions bound to the surface of the electron bubble associated with distinct angular momentum channels [Eqs. (67) and (68)]. The quasiparticle-ion potential is a hard sphere with $k_f R=11.17$. The insets highlight the low-energy region.

components of the Stokes tensor given in Eq. (65). In Fig. 10, we show our results for the temperature dependencies of the longitudinal (η_{xx}/η_N) and transverse (η_{xy}/η_N) forces normalized to the normal state Stokes drag η_N. The longitudinal drag force drops rapidly below T_c due to the (i) opening of the gap in the bulk excitation spectrum and (ii) resonant scattering reflected in terms of strong suppression of backscattering as shown in Fig. 8. The transverse force onsets at T_c, increases rapidly then decays at very low temperatures.

In the GL limit, $\Delta(T)/k_B T_c\sim(1-T/T_c)^{\frac{1}{2}}\ll 1$, the drag force decreases as $\eta_{xx}/\eta_N-1\propto-\Delta(T)$, while the transverse force scales as $\eta_{xy}/\eta_N\propto\Delta(T)^2\sim(1-T/T_c)$, reflecting the onset of branch conversion scattering of Bogoliubov quasiparticles. The scaling near T_c follows from the GL expansion of the cross sections given in Appendix D. The scaling of $\eta_{xy}\sim\Delta(T)^2$ agrees with that inferred from the estimate given in Eq. (1) of Ref. [23]; however, these authors include an additional small factor, $k_B T_c/E_f\sim 10^{-3}$, typically associated with normal-state particle-hole asymmetry. In our theory, particle-hole asymmetry is *generated* by branch conversion scattering and particle-hole coherence that onsets at T_c, and is reflected in the asymmetric chiral spectrum for $d\sigma^{(-)}/d\Omega_{\mathbf{k}'}(\mathbf{k}',\mathbf{k};E)$.

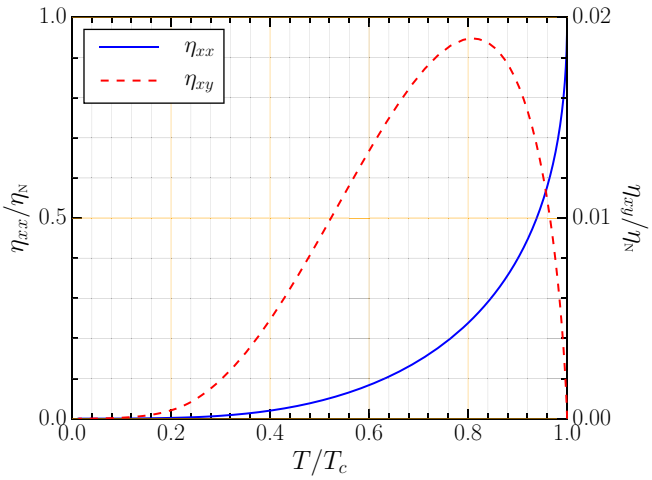

FIG. 10. Longitudinal and transverse Stokes parameters, η_{xx}/η_N (solid blue line) and η_{xy}/η_N (dashed red line), as a function of T/T_c. Calculations are based on the hard sphere quasiparticle-ion potential with $k_f R = 11.17$.

There is no factor, $k_B T_c/E_f$; however, there is a small factor originating from the small *transverse* momentum transfer that is a reflection of branch conversion scattering from the chiral order parameter. Our estimate of the longitudinal and transverse forces near T_c for an electron bubble with velocity $v\,\mathbf{e}_x$ is as follows. For the moving ion encountering a flux $n\,v$, the typical momentum transfer imparted to the ion per quasiparticle (QP) collision is $\sim p_f$, and the momentum transport cross section near T_c is $\langle\sigma_{xx}\rangle \approx \sigma_N^{\rm tr} \approx \pi R^2$, giving a drag force $|F_x| \approx n\,v\,p_f\,\sigma_N^{\rm tr}$. Now, for branch conversion scattering, there is angular momentum transfer of $\hbar$ by the chiral order parameter per branch conversion scattering of a QP. Thus the transverse momentum transfer is of order $\hbar/R$ per QP. Note that Andreev scattering is via the order parameter; there is no hard scattering with momentum transfer of order p_f. The fact that there is any momentum transfer is because of the angular momentum transfer via the chiral order parameter. In addition, branch conversion scattering onsets at T_c, thus the cross section is reduced relative to that for the longitudinal force by the probability of branch conversion scattering of thermal Bogoliubov QPs near T_c, i.e. $\langle\sigma_{xy}\rangle \approx (\Delta(T)/k_B T_c)^2\,\sigma_N^{\rm tr}$, leading to $|F_y| \approx n\,v\,(\hbar/R)\langle\sigma_{xy}\rangle \approx n\,v\,(\hbar/R)\,\sigma_N^{\rm tr}(\Delta(T)/k_B T_c)^2$, and the ratio [58]

$$\frac{|F_y|}{|F_x|} \simeq \frac{1}{k_f R}\left(\frac{\Delta(T)}{k_B T_c}\right)^2 . \tag{70}$$

The factor $1/k_f R$ accounts for the relative size of the transverse and longitudinal transport cross sections at $E \approx \Delta$ shown in Fig. 9, and also accounts for the order of magnitude reduction in the ratio η_{xy}/η_{xx} shown in Fig. 10 at $T/T_c \approx 0.8$. Note that the transport cross sections, $\sigma_{xx}(E)$ and $\sigma_{xy}(E)$, were both defined by scaling out the dimensional factors of p_f in the kinematics. Thus $\sigma_{xy}(E) \simeq \frac{\hbar}{p_f R}\sigma_{xx}(E)$ at $E \approx \Delta$. The spectral average, $\langle\sigma_{xy}(E)\rangle$ near T_c generates the additional factor of $(\Delta/k_B T_c)^2$. Although the transverse force is roughly an order of magnitude smaller than the drag force, it leads to a dramatic effect on the dynamics of the negative ion.

The equation of motion for an electron bubble under the action of an in-plane electric field is

$$M\frac{d\mathbf{v}}{dt} = e\mathbf{E} - \eta_\perp\,\mathbf{v} - \eta_{xy}\,\mathbf{v}\times\hat{\mathbf{l}}\,, \tag{71}$$

where M is the effective mass of the electron bubble. The first term on the right side of Eq. (71) is the Coulomb force on the ion, the second term is the drag force on the moving electron bubble, and the third term is the transverse force from the scattering of quasiparticles off Weyl fermions bound to the ion. The drag force results in relaxation of the ion velocity on a timescale τ given by $1/\tau = \eta_\perp/M$, while the transverse force has the form of the Lorentz force, $\mathbf{F}_{\rm W} = \frac{e}{c}\,\mathbf{v}\times\mathbf{B}_{\rm W}$, where the effective magnetic field arises from scattering of quasiparticles off the Weyl spectrum of the ion,

$$\mathbf{B}_{\rm W} = -\frac{c}{e}\eta_{xy}\,\hat{\mathbf{l}} \approx \frac{\Phi_0}{3\pi^2}\,k_f^2\,(k_f R)^2\left(\frac{\eta_{xy}}{\eta_{\rm N}}\right)\hat{\mathbf{l}}\,, \tag{72}$$

where $\Phi_0 = hc/2|e|$ is the flux quantum and we have approximated the normal state transport cross section by $\sigma_{\rm N}^{\rm tr} \approx \pi R^2$. Note that the temperature dependence of $B_{\rm W}$ is shown in Fig. 10, and thus the order of magnitude of the Weyl field ranges from $B_{\rm W} = 10^4$ T at $T/T_c = 0.8$ to $B_{\rm W} = 10^3$ T at $T/T_c = 0.3$, orders of magnitude larger that any laboratory magnetic field [9].

The Weyl field and drag force generate damped cyclotron motion of the electron bubble with frequency, $\omega_{\rm c} = eB_{\rm W}/Mc$. The resulting steady-state velocity of the electron bubble in the combined electric ($\mathbf{E} = \mathscr{E}\mathbf{e}_x$) and Weyl ($\mathbf{B}_{\rm W} = B_{\rm W}\mathbf{e}_z$) fields is given by

$$v_x = \frac{\tau}{1+(\omega_{\rm c}\tau)^2}\,e\mathscr{E}\,, \quad v_y = \frac{\tau(\omega_{\rm c}\tau)}{1+(\omega_{\rm c}\tau)^2}\,e\mathscr{E}\,. \tag{73}$$

The transverse component is the anomalous Hall current, and the ratio with the longitudinal current gives the Hall angle,

$$\tan\alpha = \frac{v_y}{v_x} = \omega_{\rm c}\tau = \frac{eB_{\rm W}}{Mc}\tau = \frac{\eta_{xy}}{\eta_\perp}\,. \tag{74}$$

Note that in spite of the enormous effective magnetic field, the Hall angle is relatively small because the relaxation time τ is so short compared to the cyclotron period, i.e. the drag force dominates the transverse force. At $T/T_c = 0.8$, where the Weyl field is maximum, the Hall angle is of order $\tan\alpha = \eta_{xy}/\eta_\perp \approx 0.1$. The detailed temperature dependencies of the Stokes parameters show that the maximum Hall angle is $\tan\alpha_{\rm max} \approx 0.25$ at $T/T_c \approx 0.4$, as shown in Fig. 12, and discussed in more detail in comparison with the experimental measurements below.

C. Comparison between theory and experiment

The experimental results for the transport of electron bubbles in ^{3}He are presented in terms of the components of the mobility tensor. The components of the mobility tensor are calculated from the Stokes parameters using Eq. (54). In Fig. 11, we compare our theoretical result for the longitudinal mobility based on numerical calculations, using the machinery presented in the previous sections, with the experimental data reported in Refs. [8,9]. The hard sphere potential works remarkably well, reproducing the longitudinal mobility data

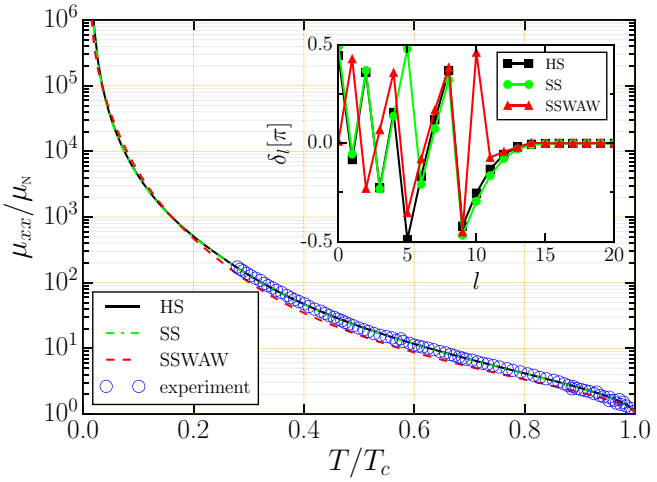

FIG. 11. Experimental data for the longitudinal mobility normalized to the normal-state mobility is from Ref. [8] shown as blue circles. The theoretical result based on the hard sphere (HS) quasiparticle-ion potential is the black curve. Results based on the soft core (SS) potential are shown as the dashed green curve, and those for the four-parameter potential with intermediate attraction (SSWAW) are shown as the red dashed curve. (Inset) Scattering phase shifts vs angular momentum channel calculated for the three potentials. For the HS model: $k_f R = 11.17$; SS model: $V_0 = 1.01\, E_f$ and $k_f R = 12.48$; SSWAW model: $V_0 = 100\, E_f$ $V_1 = 10\, E_f, k_f R' = 10.99$, and $R/R' = 0.36$, all constrained by the experimental value of μ_N.

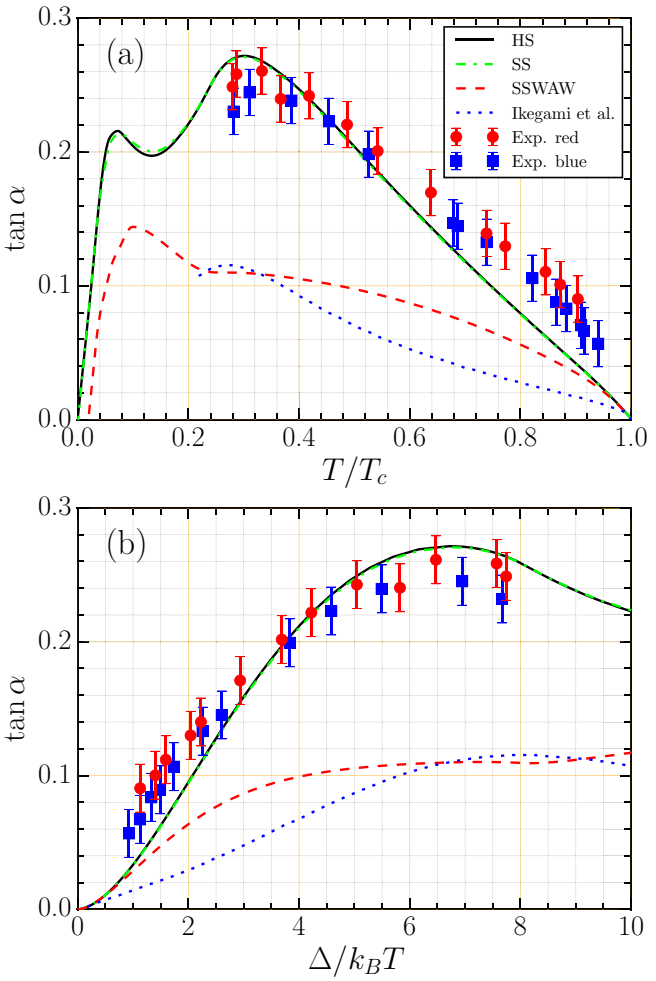

FIG. 12. (a) Hall ratio for the motion of electron bubbles in ^{3}He-A, $\tan\alpha \equiv v_y/v_x = \eta_{xy}/\eta_{xx}$, as a function of temperature for the hard sphere model for the quasiparticle-ion potential with $k_f R = 11.17$ (black line). The experimental data was from the RIKEN group [8,9]. Theoretical results for the repulsive soft core potential (dashed green line) and repulsive potential with short-range attraction (dashed red line) are shown for comparison. The dotted blue line corresponds to the calculation based on the formulas from Salmelin *et al.* [23,24] presented in Refs [8,9]. (b) The same results presented as a function of $\Delta(T)/k_BT$.

for ^{3}He-A over nearly two and a half decades for $0.25 \lesssim T/T_c \leqslant 1$. It is worth emphasizing that the hard sphere potential is a single-parameter potential with the radius, $k_f R = 11.17$, fixed by the normal-state mobility. There are no other adjustable parameters in the theory, thus the comparison between theory and experiment for μ_{xx}/μ_N is essentially perfect down to $T \approx 250\ \mu$K.

We note that Ikegami *et al.* [8] report a reasonably good comparison with their data, albeit with observable deviations at lower temperatures, using the incorrect formula for μ_{xx}/μ_N from Ref. [24] with a hard sphere radius of $k_f R = 16$. This much larger value disagrees with the radius obtained from measurements of the normal-state mobility. Moreover, as the authors of Ref. [8] found, the formula for the transverse mobility, μ_{xy}, from Ref. [24] is in serious disagreement with experimental measurements of the transverse mobility as it under estimates the Hall angle by a factor of ≈2–4 over a large temperature range, $0.25T_c \lesssim T \leqslant T_c$, based on the same value of $k_f R$. Again, the discrepancy originates from an incorrect formula for μ_{xy} reported in Ref. [24] (see Appendix A) [59].

While the comparison of our theoretical prediction for μ_{xx} is excellent agreement with the RIKEN measurements, the strong test is the comparison of our calculations for the transverse force with the measurements of the anomalous Hall effect. In Fig. 12 we show our theoretical results [solid (black) curves] for the anomalous Hall ratio given by Eq. (74), with the calculated results for η_{xy} and η_{xx} (shown in Fig. 10), plotted versus T/T_c in panel (a), and versus $\Delta(T)/k_BT$ in panel (b). The (red) circular [(blue) square] symbols correspond to the experimental data reported in Refs. [8,9]. For comparison we include the results of the calculation by Ikegami *et al.* based on the formulas from Ref. [24] as the dotted (blue) lines.

It seems worth re-emphasizing that in all our calculations reported here the only parameter is the hard sphere radius for the quasiparticle-ion potential, which is fixed at the outset as $k_f R = 11.17$ by the normal-state mobility. Thus we view the overall agreement between theory and experiment as strong confirmation of the scattering theory, particularly the origin of the anomalous Hall effect resulting from resonant scattering of thermal quasiparticles by the spectrum of Weyl fermions bound to the electron bubble embedded in ^{3}He-A.

The theoretical prediction shown in Fig. 12 shows structure in the Hall ratio—a dip-peak structure—below $T \approx 0.25\, T_c$. An important test of this theory would be measurements of the Hall mobility extended below 0.2 mK.

D. Beyond the hard sphere potential

Although the hard sphere model for the quasiparticle-ion potential provides very good agreement with the observed forces acting on the moving ion, it is only a rough approximation to expectations of the microscopic interaction between ^{3}He quasiparticles and the electron bubble. To test the robustness of our theoretical predictions to the quasiparticle-ion potential, we consider a more general central potential with short-range repulsion and intermediate-range attraction,

$$V(r) = \begin{cases} V_0, & r \leqslant R\,, \\ -V_1, & R < r \leqslant R'\,, \\ 0, & r > R'\,. \end{cases} \tag{75}$$

The normal-state scattering phase shifts for this piece-wise constant potential are expressed in terms of regular and modified spherical Bessel functions; the analytical formulas are given in Eqs. (E1)–(E3) of Appendix E. We discuss two cases both with $V_0 > E_f$: (i) for $V_1 = 0$, the potential is a two-parameter, repulsive "soft-core" potential and (ii) for $V_1 > 0$ and $R' > R$, we include in addition to the short-range repulsion, an intermediate range attraction. The latter case allows for a shallow bound state, and corresponding scattering resonance, in one or more angular momentum channels, $l \leqslant l_{\max}$.

Figures 11 and 12 show our calculations for the longitudinal mobility and Hall ratio for these potentials in comparison with the results for the hard sphere potential. The corresponding phase shifts are shown in the inset. For the "soft-core" model, we chose a weakly repulsive potential, $V_0 = 1.01\,E_f \approx 0.5$ meV, and adjusted the radius R to fit the measured normal-state mobility, $\mu_{\rm N}^{\rm exp} = 1.7\times10^{-6}\,{\rm m}^2/{\rm V/s}$, as was done for the hard-sphere potential. The resulting phase shifts, shown in inset of Fig. 11, are similar to those of calculated for hard-sphere scattering in that there are no additional strong scattering channels; the phase shift for the $l = 5$ channel corresponds to strong scattering for both the hard sphere and the soft core potential. Furthermore, there is virtually no observable change in the theoretical predictions for the longitudinal and transverse forces on the moving ion described by the soft core potential, compared to the results for the hard sphere potential. This is representative of the general class of short-range repulsive potentials. So long as the range of the repulsive quasiparticle-ion potential is adjusted to fit the normal state mobility, we obtain excellent agreement for the forces on the negative ion in the superfluid phase [60].

The situation is different for the case with short-range repulsion and intermediate range attraction. Here we fixed $V_0 = 100\,E_f$ and $V_1 = 10\,E_f$, then adjusted R and R' to obtain a best fit to the experimental value of the normal-state mobility, giving $k_f R' = 10.99$ and $R/R' = 0.36$. As can be seen from the inset of Fig. 11, the intermediate range attraction changes the set of scattering phase shifts, compared to the hard sphere potential, with the most dramatic change happening for $l = 10$. This channel exhibits an additional scattering resonance (red triangles in the inset of Fig. 11). The scattering of quasiparticles in this channel is enhanced towards the unitary limit, $\delta_{l=10} \approx \pi/2$, which makes the partial scattering cross section for this channel maximal. As a consequence, the forces on the ion are modified. The longitudinal mobility shown in Fig. 11 (red dashed line) is slightly reduced compared to that for the hard sphere scattering potential. More dramatic is the reduction in the anomalous Hall ratio shown in Fig. 12, which deviates strongly from the experimental data (red dashed line). The main conclusion here is that for the negative ion the quaiparticle-ion scattering potential is repulsive and short range, and the experimental results are well described by hard sphere potential scattering.

A softer core potential with intermediate range attraction may be relevant to understanding the mobility of positive ions in ^{3}He-A, given that the positive ion attracts ^{3}He to form a "snowball" of ^{3}He atoms with increased density relative to bulk ^{3}He [30]. Indeed preliminary measurements of the longitudinal and transverse forces on a positive ion in ^{3}He-A show different magnitudes and temperature dependencies for the longitudinal mobility and anomalous Hall ratio compared to the negative ion [9]. However, a detailed theoretical description of the structure and transport properties of the positive ion is outside the scope of this report.

VI. DISCUSSION

The comparison between theory and experiment for the Hall ratio shows a maximum deviation of ≈15% at $T \approx 0.8T_c$, which is the temperature at which the transverse force, η_{xy}, is a maximum. This suggests that there may be an additional contribution to the transverse force on the moving ion. Within the theory of thermal quasiparticles scattering off the moving ion, the larger experimental value for η_{xy} suggests an additional weak scattering mechanism contributing to the transport cross section, $\sigma_{xy}(E)$, at energies close to the gap edge, or perhaps deviations from the hard sphere potential. These possibilities for an additional contribution to the transverse force on the moving ion are addressed in a separate report.

It is also likely that in the low temperature limit, $T < 0.25T_c$, new physics appears in the transport of electron bubbles in ^{3}He-A. In particular, the theoretical prediction of the sub-gap spectrum shown in Fig. 11 leads to the sharp increase in the longitudinal mobility at low temperatures. Thus, at constant electric field we expect the linear theory for the Stokes force tensor to fail at sufficiently low temperatures as there is insufficient drag force from thermal quasiparticles to limit the ion velocity below the Landau critical velocity, $v_c = \Delta/p_f$. At high velocity the ion will dissipate energy by Cherenkov radiation of quasiparticles [61]. This process may onset at velocities well below v_c given the low energy Weyl spectrum near the moving ion, and it is an open question as to whether and how the resulting quasiparticle radiation might contribute to transverse force.

ACKNOWLEDGMENTS

The research of OS and JAS was supported by the National Science Foundation (Grant DMR-1508730). We acknowledge key discussions with Hiroki Ikegami, Kimitoshi Kono and Yasumasa Tsutsumi on the RIKEN electron mobility experiments that provided the motivation for this study. We thank Vladimir Mineev for discussions on the magnitude and interpretation of the origin of the transverse force.

APPENDIX A: CRITIQUE OF SALMELIN AND SALOMAA'S THEORY

The report by Salmelin and Salomaa (SS) on the mobility of electron bubbles in superfluid ^{3}He-A was an attempt to extend the earlier work by Salomaa *et al.* [22] on the same topic to calculate the transverse component of the mobility, μ_{xy}. The latter was argued in Ref. [23] to exist based on the analogy of the Magnus effect for a spinning object moving through a fluid, in this case the electron bubble with bound circulating currents. While the physical argument in Ref. [23] for the transverse component of the mobility is sound, the formulation of the scattering theory by Salmelin *et al.* [23,24] cannot account for the transverse force on a moving electron bubble.

The primary error introduced by Salmelin *et al.* [23,24] in their formulation of the transport cross section for an electron bubble moving in superfluid ^{3}He-A is the assumption of microscopic reversibility for scattering rates for the transition $\mathbf{k} \to \mathbf{k}'$ and the inverse scattering event, $\mathbf{k}' \to \mathbf{k}$, i.e. that $W(\mathbf{k}',\mathbf{k}) = W(\mathbf{k},\mathbf{k}')$. However, ^{3}He-$A$ breaks mirror symmetry in any plane containing the chiral axis $\hat{\mathbf{l}}$, as well as time-reversal symmetry. Thus, the condition on the scattering rate for quasiparticles scattering off an ion in ^{3}He-A connects the two scattering events for mirror reflected ground states, i.e. $W(\mathbf{k}',\hat{\mathbf{k}};+\hat{\mathbf{l}}) = W(\mathbf{k},\mathbf{k}';-\hat{\mathbf{l}})$. Conversely, microscopic reversibility is violated for the broken symmetry ground state with fixed chirality $+\hat{\mathbf{l}}$.

By assuming microscopic reversibility the authors of Ref. [24] presupposed mirror symmetry in the scattering of quasiparticles off the electron bubble, and thus ensured that the Stokes tensor is symmetric and diagonal, i.e. that $\eta_{xy} = 0$. This conclusion is clear from Eqs. (3), (5), and (6) of Salmelin *et al.* [24], and in the paragraph preceding Eqs. (4) of Ref. [23]. It is worth noting that the same assumption was made in the earlier work of Salomaa *et al.* [22] for which there was no mention or calculation of a transverse force on the moving ion.

So, why do SS obtain a nonzero result for the transverse mobility? They introduce a second error in the evaluation of the kinematic factors, $(\hat{\mathbf{k}}' - \hat{\mathbf{k}})_i(\hat{\mathbf{k}}' - \mathbf{k})_j$ ($\Delta\mathbf{p}_i\,\Delta\mathbf{p}_j$ in the notation of SS). Specifically, equations (11) in SS are incorrect in their entirety. The argument in the paragraph preceding these formulas is the source of the error. SS generated Eq. (11) by first assuming $\hat{\mathbf{k}} = \hat{\mathbf{e}}_x$ is fixed in the laboratory coordinate system such that the azimuthal angle $\phi_{\mathbf{k}} = 0$. Then, the azimuthal angle for the final state momentum, $\mathbf{k}'$, was replaced by $\phi_{\mathbf{k}'} \to \phi_{\mathbf{k}'} - \phi_{\mathbf{k}}$ to arrive at SS's Eq. (11). This procedure is invalid, but has the effect of violating mirror symmetry in the kinematics. All kinematic factors, $\Delta\hat{\mathbf{k}}_i\,\Delta\hat{\mathbf{k}}_j$, are invariant under the mirror operation $\mathbf{k} \leftrightarrow \mathbf{k}'$, in particular, $(\hat{\mathbf{k}}' - \hat{\mathbf{k}})_x(\hat{\mathbf{k}}' - \hat{\mathbf{k}})_y$ is invariant under $\mathbf{k} \leftrightarrow \mathbf{k}'$, or equivalently under $\phi_{\mathbf{k}} \leftrightarrow \phi_{\mathbf{k}'}$. Equation (11) of SS for $\Delta\hat{\mathbf{k}}_x\,\Delta\hat{\mathbf{k}}_y$ violates mirror symmetry.

The result is a spurious transverse force from a mirror symmetric scattering rate. The violation of the mirror symmetry in the kinematic factors also predicts a spurious anisotropy of the drag force in the x-y plane, i.e. $\mu_{xx} \neq \mu_{yy}$, even in the isotropic normal Fermi liquid. The authors recognized the violation of the axial symmetry of A-phase excitation gap, so they enforced a single in-plane drag coefficient by replacing $\Delta\hat{\mathbf{k}}_x\,\Delta\hat{\mathbf{k}}_x \to \frac{1}{2}(\Delta\hat{\mathbf{k}}_x\,\Delta\hat{\mathbf{k}}_x + \Delta\hat{\mathbf{k}}_y\,\Delta\hat{\mathbf{k}}_y)$ in the calculation of $\mu_\perp^{-1}$.

The erroneous set of Eqs. (11) in SS for the momentum transfer factors invalidates all the calculations of cross sections and components of the mobility tensor in Ref. [24] as well as Eqs. (4) in Ref. [23], and thus the source and magnitude of the transverse force on the moving electron bubble. In particular, the theory of SS, when evaluated with the correct formulas for the kinematic factors, $\Delta\hat{\mathbf{k}}_i\,\Delta\hat{\mathbf{k}}_j$ yields only uniaxial Stokes drag forces and zero transverse force on the moving ion, as was originally obtained in Ref. [22].

Our formulation of the force on the moving ion incorporates broken time reversal and mirror symmetries by the ^{3}He-A ground state correctly. We are able to identify scattering events that contribute to the Stokes drag and the transverse force as $W^{(+)}(\mathbf{k}',\mathbf{k}) = +W^{(+)}(\mathbf{k},\mathbf{k}')$ and $W^{(-)}(\mathbf{k}',\mathbf{k}) = -W^{(-)}(\mathbf{k},\mathbf{k}')$, respectively. Mirror symmetric scattering generates the drag forces, while the antisymmetric component to the rate is responsible for the transverse force and the anomalous Hall effect, as we discuss in Sec. IV C.

APPENDIX B: KERNEL FOR THE LDOS NEAR THE ELECTRON BUBBLE

The kernel $K^m_{l'l}(u',u,\varepsilon)$ (37), defining the LDOS and the current density, is obtained from the trace of the Nambu Green's function $\widehat{\mathscr{G}}^{\rm R}_{\rm S}(\mathbf{r},\mathbf{r};E)$ in Eqs. (31)–(33). Only the t matrix term in Eq. (33) contributes to the kernel, in which case we are led to evaluate the integral

$$\mathrm{I} = \int \frac{d^3k'}{(2\pi)^3} \int \frac{d^3k}{(2\pi)^3} e^{i(\mathbf{k}'-\mathbf{k})\cdot\mathbf{r}} \widehat{G}^{\rm R}_{\rm S}(\mathbf{k}',E)\widehat{T}^{\rm R}_{\rm S}(\mathbf{k}',\mathbf{k};E)\widehat{G}^{\rm R}_{\rm S}(\mathbf{k},E). \tag{B1}$$

We use Eq. (32) and utilize the expansion of the plane wave, $e^{i\mathbf{k}\cdot\mathbf{r}} = 4\pi \sum_{l=0}^{\infty}\sum_{m=-l}^{l} i^l\, j_l(kr) Y^m_l(\hat{\mathbf{k}})Y^m_l(\hat{\mathbf{r}})^*$, in spherical harmonics and the regular spherical Bessel functions. In the quasiclassical limit, $E_f \ll \Delta$ (see Ref. [43]), we evaluate the t matrix in the elastic limit for momenta on Fermi surface and obtain

$$\begin{aligned}\mathrm{I} = (4\pi N_f)^2 &\sum_{l,l'=0}^{\infty}\sum_{m'=-l'}^{l'}\sum_{m=-l}^{l} i^{l'-l} Y^{m'}_{l'}(\hat{\mathbf{r}})^* Y^m_l(\hat{\mathbf{r}}) \\ &\times \int \frac{d\Omega_{\mathbf{k}'}}{4\pi} \int \frac{d\Omega_{\mathbf{k}}}{4\pi} Y^{m'}_{l'}(\hat{\mathbf{k}}')Y^m_l(\hat{\mathbf{k}})^* \\ &\times \left[\int_{-\infty}^{\infty} d\xi'\, j_{l'}(k'r)\widehat{G}^{\rm R}_{\rm S}(\mathbf{k}',E)\right]\widehat{T}^{\rm R}_{\rm S}(\hat{\mathbf{k}}',\hat{\mathbf{k}};E) \\ &\times \left[\int_{-\infty}^{\infty} d\xi\, j_l(kr)\widehat{G}^{\rm R}_{\rm S}(\mathbf{k},E)\right].\end{aligned} \tag{B2}$$

The remaining integral

$$\mathrm{J} = \int_{-\infty}^{\infty} d\xi\, j_l(kr)\widehat{G}^{\rm R}_{\rm S}(\mathbf{k},E) \tag{B3}$$

is evaluated most conveniently using spherical Hankel functions of the first and second kind,

$$h^{(1,2)}_l(x) = j_l(x) \pm i n_l(x), \quad \text{where} \quad h^{(1,2)}_l(x) \propto e^{\pm ix}, \tag{B4}$$

in which case we obtain

$$\mathrm{J} = \frac{1}{2}\big[h_l^{(1)}(k_f r)\,\mathrm{J}^{+} + h_l^{(2)}(k_f r)\,\mathrm{J}^{-}\big]\,, \tag{B5}$$

$$\mathrm{J}^{\pm} \equiv \int d\xi\; e^{\pm i\frac{\xi}{\hbar v_f} r}\;\widehat{G}^{\mathrm{R}}_{\mathrm{S}}(\mathbf{k},E)\,, \tag{B6}$$

where we used $k = k_f + \xi/\hbar v_f$. The integrals $\mathrm{J}^{\pm}$ are evaluated using Eq. (16),

$$\mathrm{J}^{\pm} = -i\pi e^{-\sqrt{|\Delta(\hat{\mathbf{k}})|^2-\varepsilon^2}\frac{r}{\hbar v_f}}\left[\frac{-i}{\sqrt{|\Delta(\hat{\mathbf{k}})|^2-\varepsilon^2}}\begin{pmatrix}\varepsilon\mathbb{1} & -\hat{\Delta}(\hat{\mathbf{k}})\\ -\hat{\Delta}^{\dagger}(\hat{\mathbf{k}}) & \varepsilon\mathbb{1}\end{pmatrix} \pm \begin{pmatrix}\mathbb{1} & 0\\ 0 & -\mathbb{1}\end{pmatrix}\right]. \tag{B7}$$

Expressing the spherical harmonics as $Y_l^m(\hat{\mathbf{k}}) \equiv Y_l^m(\theta,\phi) = \Theta_l^m(\cos\theta)\,e^{im\phi}$, we then integrate over the azimuthal angles in Eq. (B2). Finally, Eq. (36) is obtained by evaluating the trace over the Nambu matrices in Eq. (B2),

$$\sum_{m=-\infty}^{\infty}\delta N_m(\mathbf{r},E) = -\frac{1}{2\pi}\mathrm{Im}[\mathrm{Tr}(\mathrm{I})]. \tag{B8}$$

APPENDIX C: FORMULAE FOR THE ELECTRON BUBBLE CURRENT DENSITY

The current density circulating an electron bubble in cartesian components is $\mathbf{j}(r,\vartheta,\varphi) = \sum_{i=x,y,z} j_i(\mathbf{r})\,\hat{\mathbf{e}}_i$. The current along the chiral axis,

$$j_z(\mathbf{r}) = -4\pi^3 v_f N_f k_B T\,\mathrm{Re}\Bigg\{\sum_{n=0}^{\infty}\sum_{m=-\infty}^{\infty}\sum_{l,l'=|m|}^{\infty}\Theta_{l'}^m(\cos\vartheta)\Theta_l^m(\cos\vartheta)\int_{-1}^{1}du'\int_{-1}^{1}du(u'+u)$$
$$\times\,\Theta_{l'}^m(u')e^{-\sqrt{\Delta^2(1-u'^2)+\varepsilon_n^2}\frac{r}{\hbar v_f}}\Theta_l^m(u)e^{-\sqrt{\Delta^2(1-u^2)+\varepsilon_n^2}\frac{r}{\hbar v_f}}K_{l'l}^m(u',u,i\varepsilon_n)\Bigg\}\,, \tag{C1}$$

vanishes by symmetry; in particular, the spectrum of Weyl fermions is symmetric under $z\to -z$. The in-plane components are expressed in terms for the four terms related to the components of the t matrix,

$$j_x(\mathbf{r}) = -4\pi^3 v_f N_f k_B T\,\mathrm{Re}\Bigg\{\sum_{n=0}^{\infty}\sum_{m=-\infty}^{\infty}\frac{1}{2}\big[j_1^m(\mathbf{r},\varepsilon_n)+j_2^m(\mathbf{r},\varepsilon_n)+j_3^m(\mathbf{r},\varepsilon_n)+j_4^m(\mathbf{r},\varepsilon_n)\big]\Bigg\}\,, \tag{C2}$$

$$j_y(\mathbf{r}) = -4\pi^3 v_f N_f k_B T\,\mathrm{Re}\Bigg\{\sum_{n=0}^{\infty}\sum_{m=-\infty}^{\infty}\frac{1}{2i}\big[j_1^m(\mathbf{r},\varepsilon_n)-j_2^m(\mathbf{r},\varepsilon_n)+j_3^m(\mathbf{r},\varepsilon_n)-j_4^m(\mathbf{r},\varepsilon_n)\big]\Bigg\}, \tag{C3}$$

where

$$j_1^m(\mathbf{r},\varepsilon_n) = e^{i\varphi}\sum_{l'=|m-1|}^{\infty}\sum_{l=|m|}^{\infty}\Theta_{l'}^{m-1}(\cos\vartheta)\Theta_l^m(\cos\vartheta)\int_{-1}^{1}du'\int_{-1}^{1}du\sqrt{1-u'^2}$$
$$\times\,\Theta_{l'}^{m-1}(u')e^{-\sqrt{\Delta^2(1-u'^2)+\varepsilon_n^2}\frac{r}{\hbar v_f}}\Theta_l^m(u)e^{-\sqrt{\Delta^2(1-u^2)+\varepsilon_n^2}\frac{r}{\hbar v_f}}K_{l'l}^m(u',u,i\varepsilon_n)\,, \tag{C4}$$

$$j_2^m(\mathbf{r},\varepsilon_n) = e^{-i\varphi}\sum_{l'=|m+1|}^{\infty}\sum_{l=|m|}^{\infty}\Theta_{l'}^{m+1}(\cos\vartheta)\Theta_l^m(\cos\vartheta)\int_{-1}^{1}du'\int_{-1}^{1}du\sqrt{1-u'^2}$$
$$\times\,\Theta_{l'}^{m+1}(u')e^{-\sqrt{\Delta^2(1-u'^2)+\varepsilon_n^2}\frac{r}{\hbar v_f}}\Theta_l^m(u)e^{-\sqrt{\Delta^2(1-u^2)+\varepsilon_n^2}\frac{r}{\hbar v_f}}K_{l'l}^m(u',u,i\varepsilon_n), \tag{C5}$$

$$j_3^m(\mathbf{r},\varepsilon_n) = e^{i\varphi}\sum_{l'=|m|}^{\infty}\sum_{l=|m+1|}^{\infty}\Theta_{l'}^{m}(\cos\vartheta)\Theta_l^{m+1}(\cos\vartheta)\int_{-1}^{1}du'\int_{-1}^{1}du\sqrt{1-u^2}$$
$$\times\,\Theta_{l'}^{m}(u')e^{-\sqrt{\Delta^2(1-u'^2)+\varepsilon_n^2}\frac{r}{\hbar v_f}}\Theta_l^{m+1}(u)e^{-\sqrt{\Delta^2(1-u^2)+\varepsilon_n^2}\frac{r}{\hbar v_f}}K_{l'l}^m(u',u,i\varepsilon_n), \tag{C6}$$

$$j_4^m(\mathbf{r},\varepsilon_n) = e^{-i\varphi}\sum_{l'=|m|}^{\infty}\sum_{l=|m-1|}^{\infty}\Theta_{l'}^m(\cos\vartheta)\Theta_l^{m-1}(\cos\vartheta)\int_{-1}^{1}du'\int_{-1}^{1}du\sqrt{1-u^2}$$
$$\times\,\Theta_{l'}^m(u')e^{-\sqrt{\Delta^2(1-u'^2)+\varepsilon_n^2}\frac{r}{\hbar v_f}}\Theta_l^{m-1}(u)e^{-\sqrt{\Delta^2(1-u^2)+\varepsilon_n^2}\frac{r}{\hbar v_f}}K_{l'l}^m(u',u,i\varepsilon_n). \tag{C7}$$

Using the following symmetry properties of the kernel, $K_{l'l}^m(u',u,i\varepsilon_n)\equiv i^{l'-l}\kappa_{l'l}^m(u',u,i\varepsilon_n)$,

$$\kappa_{l'l}^{-m}(u',u,i\varepsilon_n) = -\left[\kappa_{l'l}^m(u',u,i\varepsilon_n)\right]^*, \tag{C8}$$

$$\kappa_{ll'}^m(u,u',i\varepsilon_n) = \kappa_{l'l}^m(u',u,i\varepsilon_n), \tag{C9}$$

one finds that the current density is purely azimuthal, $\mathbf{j}(r,\vartheta,\varphi) = j_\varphi(r,\vartheta)\,\mathbf{e}_\varphi$,with $\mathbf{e}_\varphi = -\sin\varphi\mathbf{e}_x + \cos\varphi\mathbf{e}_y$,

$$j_\varphi(r,\vartheta) = -8\pi^3 v_f N_f k_B T\sum_{n=0}^{\infty}\sum_{m=-\infty}^{\infty}\sum_{l'=|m-1|}^{\infty}\sum_{l=|m|}^{\infty}\Theta_{l'}^{m-1}(\cos\vartheta)\Theta_l^m(\cos\vartheta)\int_{-1}^{1}du'\int_{-1}^{1}du\sqrt{1-u'^2}$$
$$\times\,\Theta_{l'}^{m-1}(u')e^{-\sqrt{\Delta^2(1-u'^2)+\varepsilon_n^2}\frac{r}{\hbar v_f}}\Theta_l^m(u)e^{-\sqrt{\Delta^2(1-u^2)+\varepsilon_n^2}\frac{r}{\hbar v_f}}\mathrm{Re}\left[\kappa_{l'l}^m(u',u,i\varepsilon_n)\right]\mathrm{Im}[i^{l'-l}]. \tag{C10}$$

APPENDIX D: FORMULAE FOR THE SCATTERING RATE AND TRANSPORT CROSS SECTION

We summarize our results for the transport cross sections in terms of the solutions to the coupled Eqs. (25)–(28) for the t matrix. Given the solutions for the branch components, t_a^m, we substitute Eqs. (25)–(28) into Eq. (60), to obtain

$$W(\hat{\mathbf{k}}',\hat{\mathbf{k}}) = \frac{1}{\pi^2 N_F^2}\sum_{m=-\infty}^{\infty}\sum_{m'=-\infty}^{\infty}e^{-i(m'-m)(\phi'-\phi)}$$
$$\times\left\{\left[t_1^m(u',u)^* + (-1)^{m+1}\frac{\Delta\sqrt{1-u^2}}{E}e^{-i(\phi'-\phi)}t_2^m(u',-u)^*\right]\times\left[t_1^{m'}(u',u) + (-1)^{m'}\frac{\Delta\sqrt{1-u'^2}}{E}t_3^{m'}(-u',u)\right]\right.$$
$$+\left[(-1)^{m+1}t_2^m(u',-u)^* + \frac{\Delta\sqrt{1-u^2}}{E}e^{i(\phi'-\phi)}t_1^m(u',u)^*\right]\times\left[(-1)^{m'+1}t_2^{m'}(u',-u) + \frac{\Delta\sqrt{1-u'^2}}{E}t_4^{m'}(-u',-u)\right]$$
$$+\left[(-1)^m t_3^m(-u',u)^* + \frac{\Delta\sqrt{1-u^2}}{E}e^{-i(\phi'-\phi)}t_4^m(-u',-u)^*\right]\times\left[(-1)^{m'}t_3^{m'}(-u',u) + \frac{\Delta\sqrt{1-u'^2}}{E}t_1^{m'}(u',u)\right]$$
$$\left.+\left[t_4^m(-u',-u)^* + (-1)^m\frac{\Delta\sqrt{1-u^2}}{E}e^{i(\phi'-\phi)}t_3^m(-u',u)^*\right]\times\left[t_4^{m'}(-u',-u) + (-1)^{m'+1}\frac{\Delta\sqrt{1-u'^2}}{E}t_2^{m'}(u',-u)\right]\right\}. \tag{D1}$$

A key feature of the scattering rate is the dependence on the azimuthal angles for the incident and outgoing momenta *only* in the combination $(\phi'-\phi)$. This greatly simplifies the calculation of the transport cross sections [see Eqs. (67) and (68)], since any other combination of ϕ' and ϕ gives zero contribution after integration over incident and final state momenta. This allows us to show the following:

$$\sigma_{xy}^{(+)}(E) = \sigma_{yx}^{(+)}(E) = 0, \tag{D2}$$

$$\sigma_{xz}^{(\pm)}(E) = \sigma_{zx}^{(\pm)}(E) = \sigma_{yz}^{(\pm)}(E) = \sigma_{zy}^{(\pm)}(E) = 0, \tag{D3}$$

$$\sigma_{xx}^{(+)}(E) = \sigma_{yy}^{(+)}(E), \tag{D4}$$

$$\sigma_{xy}^{(-)}(E) = -\sigma_{yx}^{(-)}(E). \tag{D5}$$

To carry out calculations, we project out scattering rates with different orbital angular momenta, $\Delta m = 0,\pm1$,

$$\frac{2\pi}{k_F^2}W_0(u',u) = \left(\frac{m^*}{2\pi\hbar^2}\right)^2\int_0^{2\pi}d\phi\int_0^{2\pi}\frac{d\phi'}{2\pi}W(\hat{\mathbf{k}}',\hat{\mathbf{k}}), \tag{D6}$$

$$\frac{2\pi}{k_F^2}W_\pm(u',u) = \left(\frac{m^*}{2\pi\hbar^2}\right)^2\int_0^{2\pi}d\phi\int_0^{2\pi}\frac{d\phi'}{2\pi}e^{\pm i(\phi'-\phi)}W(\hat{\mathbf{k}}',\hat{\mathbf{k}}). \tag{D7}$$

These rates are expressed in terms of the solutions to the t matrix amplitudes,

$$
\begin{aligned}
&W_0(u',u)\\
&= \sum_{m=-\infty}^{\infty}\Bigg\{\left[t_1^m(u',u)^* + (-1)^m\frac{\Delta\sqrt{1-u^2}}{E}t_2^{m+1}(u',-u)^*\right]\times\left[t_1^m(u',u) + (-1)^m\frac{\Delta\sqrt{1-u'^2}}{E}t_3^m(-u',u)\right]\\
&\quad+\left[(-1)^{m+1}t_2^m(u',-u)^* + \frac{\Delta\sqrt{1-u^2}}{E}t_1^{m-1}(u',u)^*\right]\times\left[(-1)^{m+1}t_2^m(u',-u) + \frac{\Delta\sqrt{1-u'^2}}{E}t_4^m(-u',-u)\right]\\
&\quad+\left[(-1)^m t_3^m(-u',u)^* + \frac{\Delta\sqrt{1-u^2}}{E}t_4^{m+1}(-u',-u)^*\right]\times\left[(-1)^m t_3^m(-u',u) + \frac{\Delta\sqrt{1-u'^2}}{E}t_1^m(u',u)\right]\\
&\quad+\left[t_4^m(-u',-u)^* + (-1)^{m-1}\frac{\Delta\sqrt{1-u^2}}{E}t_3^{m-1}(-u',u)^*\right]\times\left[t_4^m(-u',-u) + (-1)^{m+1}\frac{\Delta\sqrt{1-u'^2}}{E}t_2^m(u',-u)\right]\Bigg\},
\end{aligned}
\tag{D8}
$$

$$
\begin{aligned}
&W_\pm(u',u)\\
&= \sum_{m=-\infty}^{\infty}\Bigg\{\left[t_1^{m\mp1}(u',u)^* + (-1)^{m\mp1}\frac{\Delta\sqrt{1-u^2}}{E}t_2^{m\mp1+1}(u',-u)^*\right]\times\left[t_1^m(u',u) + (-1)^m\frac{\Delta\sqrt{1-u'^2}}{E}t_3^m(-u',u)\right]\\
&\quad+\left[(-1)^{m\mp1+1}t_2^{m\mp1}(u',-u)^* + \frac{\Delta\sqrt{1-u^2}}{E}t_1^{m\mp1-1}(u',u)^*\right]\times\left[(-1)^{m+1}t_2^m(u',-u) + \frac{\Delta\sqrt{1-u'^2}}{E}t_4^m(-u',-u)\right]\\
&\quad+\left[(-1)^{m\mp1}t_3^{m\mp1}(-u',u)^* + \frac{\Delta\sqrt{1-u^2}}{E}t_4^{m\mp1+1}(-u',-u)^*\right]\times\left[(-1)^m t_3^m(-u',u) + \frac{\Delta\sqrt{1-u'^2}}{E}t_1^m(u',u)\right]\\
&\quad+\left[t_4^{m\mp1}(-u',-u)^* + (-1)^{m\mp1-1}\frac{\Delta\sqrt{1-u^2}}{E}t_3^{m\mp1-1}(-u',u)^*\right]\\
&\quad\times\left[t_4^m(-u',-u) + (-1)^{m+1}\frac{\Delta\sqrt{1-u'^2}}{E}t_2^m(u',-u)\right]\Bigg\}.
\end{aligned}
\tag{D9}
$$

Formulae for the in-plane transport cross sections are given in terms of integrations over $W_{0,\pm}(u',u;E)$,

$$
\begin{aligned}
\sigma_{xx}^{(+)}(E) &= \frac{3\pi}{4k_F^2}\int_{E\geqslant|\Delta(\hat{\mathbf{k}})|}du\int_{E\geqslant|\Delta(\hat{\mathbf{k}}')|}du'\frac{E^2}{\sqrt{E^2-|\Delta(\hat{\mathbf{k}})|^2}\sqrt{E^2-|\Delta(\hat{\mathbf{k}}')|^2}}\\
&\quad\times\left\{\left(1-\frac{u^2+u'^2}{2}\right)W_0(u',u) - \frac{1}{2}\sqrt{1-u^2}\sqrt{1-u'^2}[W_+(u',u)+W_-(u',u)]\right\},
\end{aligned}
\tag{D10}
$$

$$
\begin{aligned}
\sigma_{xy}^{(-)}(E) &= \frac{3\pi}{4k_F^2}\int_{E\geqslant|\Delta(\hat{\mathbf{k}})|}du\int_{E\geqslant|\Delta(\hat{\mathbf{k}}')|}du'\frac{E^2}{\sqrt{E^2-|\Delta(\hat{\mathbf{k}})|^2}\sqrt{E^2-|\Delta(\hat{\mathbf{k}}')|^2}}\\
&\quad\times\left\{\frac{1-2f}{4i}\sqrt{1-u^2}\sqrt{1-u'^2}[W_+(u',u)-W_-(u',u)+W_+(u,u')-W_-(u,u')]\right\}.
\end{aligned}
\tag{D11}
$$

The other elements of the tensor cross sections are obtained by the symmetry relations, Eqs. (D2)–(D5).

APPENDIX E: SCATTERING PHASE SHIFTS FOR QUASIPARTICLE-ION POTENTIALS

For the potential defined by Eq. (75), the scattering phase shifts for normal-state quasiparticles are calculated from the following expressions:

$$
\tan\delta_l = \frac{(l-\gamma_l)j_l(k_fR') - k_fR'j_{l+1}(k_fR')}{(l-\gamma_l)n_l(k_fR') - k_fR'n_{l+1}(k_fR')},\quad \gamma_l = x'\frac{a_l}{b_l},
\tag{E1}
$$

$$
\begin{aligned}
a_l &= l[n_{l+1}(x)j_l(x') - n_l(x')j_{l+1}(x)] + x'[n_{l+1}(x')j_{l+1}(x) - n_{l+1}(x)j_{l+1}(x')]\\
&\quad+\frac{lp_l}{x'}[n_l(x)j_l(x') - n_l(x')j_l(x)] + p_l[n_{l+1}(x')j_l(x) - n_l(x)j_{l+1}(x')],
\end{aligned}
\tag{E2}
$$

$$
b_l = x'[n_{l+1}(x)j_l(x') - n_l(x')j_{l+1}(x)] + p_l[n_l(x)j_l(x') - n_l(x')j_l(x)],
\tag{E3}
$$

and $p_l = z'i_{l+1}(z)/i_l(z)$ with $x=\beta_1k_fR$, $x'=\beta_1k_fR'$, $z=\beta_0k_fR$, $z'=\beta_0k_fR'$, $\beta_0=\sqrt{\frac{V_0-E_f}{E_f}}$, and $\beta_1=\sqrt{\frac{E_f+V_1}{E_f}}$, where $i_l(x)$ is the modified spherical Bessel function of the first kind.

[1] P. W. Anderson and P. Morel, Phys. Rev. Lett. **5**, 136 (1960).
[2] G. Volovik, Zh. Eksp. Teor. Fiz. Pis. Red. **22**, 234 (1975) [Sov. Phys. JETP Lett. **22**, 108 (1975)].
[3] M. C. Cross, J. Low Temp. Phys. **26**, 165 (1977).
[4] M. Ishikawa, Prog. Theor. Phys. **57**, 1836 (1977).
[5] A. J. Leggett and S. Takagi, Ann. Phys. **110**, 353 (1978).
[6] M. G. McClure and S. Takagi, Phys. Rev. Lett. **43**, 596 (1979).
[7] D. Rainer and M. Vuorio, J. Phys. C **10**, 3093 (1977).
[8] H. Ikegami, Y. Tsutsumi, and K. Kono, Science **341**, 59 (2013).
[9] H. Ikegami, Y. Tsutsumi, and K. Kono, J. Phys. Soc. Jpn. **84**, 044602 (2015).
[10] J. A. Sauls, Phys. Rev. B **84**, 214509 (2011).
[11] G. E. Volovik and V. P. Mineev, Zh. Eksp. Teor. Fiz. **81**, 989 (1981) [Sov. Phys JETP **54**, 524 (1981)].
[12] Y. Hatsugai, Phys. Rev. Lett. **71**, 3697 (1993).
[13] G. E. Volovik, arXiv:1602.02595.
[14] T. Mizushima, Y. Tsutsumi, T. Kawakami, M. Sato, M. Ichioka, and K. Machida, J. Phys. Soc. Jpn. **85**, 022001 (2016).
[15] N. Read and D. Green, Phys. Rev. B **61**, 10267 (2000).
[16] G. E. Volovik, Zh. Eksp. Teor. Fiz. **94**, 123 (1988) [Sov. Phys. JETP **67**, 1804 (1988)].
[17] G. E. Volovik, Pis'ma Zh. Eksp. Teor. Fiz. **55**, 363 (1992) [JETP Lett. **55**, 368 (1992)].
[18] G. E. Volovik, *Exotic Properties of Superfluid* ^{3}He (World Scientific, Singapore, 1992).
[19] M. Stone and R. Roy, Phys. Rev. B **69**, 184511 (2004).
[20] This is a sheet current obtained by integrating the current density confined on the boundary.
[21] Y. Tsutsumi and K. Machida, Phys. Rev. B **85**, 100506 (2012).
[22] M. Salomaa, C. J. Pethick, and G. Baym, Phys. Rev. Lett. **44**, 998 (1980).
[23] R. H. Salmelin, M. M. Salomaa, and V. P. Mineev, Phys. Rev. Lett. **63**, 868 (1989).
[24] R. H. Salmelin and M. M. Salomaa, Phys. Rev. B **41**, 4142 (1990).
[25] For a historical review of theories of the anomalous Hall effect in solid state systems, see N. A. Sinitsyn, J. Phys.: Condens. Matter **20**, 023201, (2008).
[26] M. A. Woolf and G. W. Rayfield, Phys. Rev. Lett. **15**, 235 (1965).
[27] R. A. Ferrell, Phys. Rev. **108**, 167 (1957).
[28] C. G. Kuper, Phys. Rev. **122**, 1007 (1961).
[29] A. L. Fetter, in *The Physics of Liquid and Solid Helium*, edited by K. Benneman and J. Ketterson (John Wiley & Sons, New York, 1976), Vol. 1, pp. 207–305.
[30] E. R. Dobbs, *Helium Three* (Oxford University Press, Oxford, England, 2000).
[31] A. I. Ahonen, J. Kokko, M. A. Paalanen, R. C. Richardson, W. Schoepe, and Y. Takano, J. Low Temp. Phys. **30**, 205 (1978).
[32] D. R. LoveJoy, Can. J. Phys. **33**, 49 (1955).
[33] M. Suzuki, Y. Okuda, A. J. Ikushima, and M. Iino, Europhys. Lett. **5**, 333 (1988).
[34] B. D. Josephson and J. Lekner, Phys. Rev. Lett. **23**, 111 (1969).
[35] A. L. Fetter and J. Kurkijärvi, Phys. Rev. B **15**, 4272 (1977).
[36] A. Messiah, *Quantum Mechanics* (North-Holland, Amsterdam, 1958), Vol. I.
[37] A quantitative physical explanation for the difference in these different determinations of the size of the electron bubble has not been presented. One possible source of the discrepancy is the assumption implied by the analysis based on Eq. (1) that the surface tension, γ, determined in the hydrostatic limit can be extended to curvatures of order $R \simeq 2$ nm.
[38] G. Baym, C. J. Pethick, and M. Salomaa, Phys. Rev. Lett. **38**, 845 (1977).
[39] E. Thuneberg, J. Kurkijärvi, and D. Rainer, J. Phys. C **14**, 5615 (1981).
[40] J. W. Serene and D. Rainer, Phys. Rep. **101**, 221 (1983).
[41] J. Mathews and R. L. Walker, *Mathematical Methods of Physics* (W. H. Benjamin Inc., New York, 1965).
[42] Equation (18) is formulated for all energies and momenta of the incident and final-state excitations. We require the on-shell t matrix in the low-energy region near the Fermi surface. High-energy intermediate states are included in the phase shifts defining the normal-state t matrix and can be evaluated for momenta on the Fermi surface and $E = 0$. We note that physical quantities, like the mobility or transport cross section, are determined by $\hat{T}_S^R(\hat{k}', \hat{k})$ with an additional constraint, $E \geqslant |\Delta(\hat{k})|$ and $E \geqslant |\Delta(\hat{k}')|$, see Eqs. (66)–(68). Strictly speaking, only these matrix elements are "on-shell" since there are no bulk quasiparticle states with momentum $\mathbf{k}$ for $E < |\Delta(\hat{\mathbf{k}})|$. Nevertheless, Eq. (19) contains both off-shell and on-shell matrix elements. After solving this equation we retain only the on-shell matrix elements.
[43] $\int d^3k/(2\pi)^3(\ldots) \approx N_f \int d\Omega_{\mathbf{k}}/4\pi \int d\xi_k(\ldots)$.
[44] The propagator for bulk A phase [Eq. (16)] gives zero current density, and thus zero angular momentum density, when evaluated in the quasiclassical limit with particle-hole symmetry of the normal-state spectrum. This is consistent with earlier calculations for the bulk angular momentum density for uniform superfluid ^{3}He-A, cf. Ref. [11].
[45] A. Abrikosov, L. Gorkov, and I. Dzyaloshinski, *Methods of Quantum Field Theory in Statistical Physics*, 2nd ed. (Pergamon, Oxford, 1965).
[46] This result is at odds with the GL theory result of Rainer and Vuorio [7], who found the circulating currents generated by an impurity in ^{3}He-A, but with zero net angular momentum. Their GL calculation for the current and angular momentum is restricted to the asymptotic region, $r \gg \xi_0$, where we find the current density is 4–5 orders of magnitude smaller than that in the mesoscopic region $R < r \lesssim \xi_0$.
[47] A. C. Anderson, M. Kuchnir, and J. C. Wheatley, Phys. Rev. **168**, 261 (1968).
[48] R. M. Bowley, J. Phys. C **10**, 4033 (1977).
[49] A. I. Ahonen, J. Kokko, O. V. Lounasmaa, M. A. Paalanen, R. C. Richardson, W. Schoepe, and Y. Takano, Phys. Rev. Lett. **37**, 511 (1976).
[50] R. H. Salmelin and M. M. Salomaa, J. Phys. C **20**, L681 (1987).
[51] J. T. Simola, K. K. Nummila, A. Hirai, J. S. Korhonen, W. Schoepe, and L. Skrbek, Phys. Rev. Lett. **57**, 1923 (1986).
[52] G. Baym, C. J. Pethick, and M. Salomaa, J. Low Temp. Phys. **36**, 431 (1979).
[53] G. Baym, R. G. Barrera, and C. J. Pethick, Phys. Rev. Lett. **22**, 20 (1969).
[54] R. G. Watts and R. Ferrer, Am. J. Phys. **55**, 40 (1987).
[55] The derivation of Eq. (68) includes a term, $\propto \int d\Omega_{\mathbf{k}'} \int d\Omega_{\mathbf{k}} (\hat{\mathbf{k}}'_i \hat{\mathbf{k}}'_j - \hat{\mathbf{k}}_i \hat{\mathbf{k}}_j) d\sigma^{(-)}/d\Omega_{\mathbf{k}'}(\hat{\mathbf{k}}', \hat{\mathbf{k}}; E)$, which, based on the analysis in Appendix D, vanishes identically.
[56] The experiments are carried out at ac frequencies from 1−10 Hz. The current response contains both an in-phase and out-of-phase

ac components, which can be calculated from the hydrodynamical equations with the M and η_{ij} calculated in the low velocity, dc limit.

[57] M. Abramowitz and I. Stegun, *Handbook of Mathematical Functions*, 10th ed. (US Government Printing Office, Washington DC, 1972).

[58] The force ratio estimate given in Eq. (70) was obtained by Vladimir Mineev based on hydrodynamic scaling in the Knudsen and GL limits (private communication). Our analysis gives the same result, and is based on our scattering theory formulation for potential scattering and branch conversion scattering.

[59] The actual discrepancy is more severe. The theory of Salmelin *et al.* in Refs. [23,24], when evaluated properly, predicts *zero transverse force*, i.e. $\mu_{xy} \equiv 0$. The expression used for calculating μ_{xy}^{-1} by the RIKEN group, Eqs. (6) and (11) from Ref. [24], is *identically zero* when evaluated with the correct angular dependence for the kinematic factor, $(\hat{\mathbf{k}}' - \hat{\mathbf{k}})_x(\hat{\mathbf{k}}' - \hat{\mathbf{k}})_y$.

[60] O. Shevtsov and J. A. Sauls, arXiv:1608.01644.

[61] J. H. Jensen and J. A. Sauls, Phys. Rev. B **38**, 13387 (1988).